Parabrachial *Calca* neurons drive nociplasticity

Logan Francis Condon

A dissertation
submitted in partial fulfillment of
the requirements for the degree of

Doctor of Philosophy

University of Washington
2024

Reading Committee:
Richard Palmiter, Chair
Ajay Dhaka
Benjamin Land

Program Authorized to Offer Degree:
Neuroscience

University of Washington

ABSTRACT

Parabrachial *Calca* neurons drive nociplasticity

Logan Francis Condon

Chair of the Supervisory Committee:

Richard Palmiter

Department of Biochemistry

Pain that persists beyond the time required for tissue healing and pain that arises in the absence of tissue injury, collectively referred to as nociplastic pain, are poorly understood phenomena mediated by plasticity within the central nervous system. The parabrachial nucleus (PBN) is a hub that relays aversive sensory information and appears to play a role in nociplasticity. Here, by preventing PBN *Calca* neurons from releasing neurotransmitter we demonstrate that activation of *Calca* neurons is necessary for the manifestation and maintenance of chronic pain. Additionally, by directly stimulating *Calca* neurons we demonstrate that *Calca* neuron activity is sufficient to drive nociplasticity. Aversive stimuli of multiple sensory modalities such as exposure to nitroglycerin, cisplatin, or LiCl can drive nociplasticity in a *Calca*-neuron-dependent manner. Aversive events drive nociplasticity in *Calca* neurons in the form of

increased activity and excitability; however, nociplasticity also appears to occur in downstream circuitry.

Table of contents

Introduction

Pain is an evolutionarily adaptive sensory modality that signals tissue injury and triggers defensive behavioral responses. However, pain sensation can also be a driver of morbidity when it persists beyond acute tissue insult and becomes chronic. Chronic pain affects one in five people (Mills et al., 2018; Dahlhamer et al., 2018; Maixner et al., 2016) and is estimated to cost the United States between $560 billion and $635 billion annually (Smith and Hillner 2019). For the past several decades, long-term opioid therapy has been the primary approach to managing chronic pain symptoms (Busse et al., 2018; Ballantyne and Shin 2008). Unfortunately, it is not clear whether long-term opioid therapy is effective at controlling chronic pain symptoms and at best, the magnitude of the effect is minimal (Busse et al., 2018; Ballantyne and Shin 2008). Long-term opioid therapy is also associated with addiction, pharmacologic tolerance, opioid-induced hyperalgesia, nausea, and several other deleterious side effects (Busse et al., 2018; Ballantyne and Shin 2008). It is imperative that we further develop our understanding of the mechanisms underlying pain sensation and the manifestation of chronic pain so that we may develop more efficacious therapies for chronic pain management.

Pain sensation is subcategorized based on its point of origin. Nociceptive pain is the result of inflammation and/or damage to non-nervous tissue, neuropathic pain is caused by damage to the peripheral or central nervous system, and nociplastic pain is the result of altered pain and sensory processing within the central nervous system (Fitzcharles et al., 2021). While all forms of pain sensation can be experienced chronically, the primary method for studying the physiology and anatomy underlying

chronic pain is to instate chronic neuropathy in a model organism (Malmberg and Basbaum, 1998).

The aim of this thesis is to contribute to our understanding of the anatomy and physiology involved in chronic pain sensation and develop a novel model for the study of chronic pain that does not rely on artificially induced neuropathy. More specifically, this thesis focuses on the role calcitonin gene-related polypeptide alpha gene (*Calca*) expressing neurons in the parabrachial nucleus (PBN) play in the manifestation of chronic nociplasticity. The results section is an adapted version of a manuscript under review for publication that delineates the necessity of *Calca* neuron activity in the manifestation of chronic pain, the sufficiency of *Calca* neuron activity in the manifestation of nociplasticity, and the neuroplasticity exhibited by *Calca* neurons following robust activation.

Central pathways underlying pain sensation

Canonically, pain sensation originates in the peripheral nervous system, where Aδ fiber and C fiber nociceptors transduce noxious stimuli (Basbaum et al., 2009; Saper et al., 2012). These nociceptors transmit noxious information to the spinal cord via synapses in the superficial lamina of the dorsal horn (Basbaum et al., 2009). Within the dorsal horn, nociceptive information follows two pathways to the forebrain. The spinothalamic pathway projects to the sensory nuclei of the thalamus and then on to the sensory cortex (Bernard et al., 1995). The spino-parabrachial pathway projects to the PBN and then on to the hypothalamus and amygdala (Bernard et al., 1995; Bourgeais er al., 2003; Choi et al., 2020). The spinothalamic circuit carries the identity of pain information (e.g., thermal, tactile, chemical, etc.) and the spino-parabrachial pathway carries the valence and intensity of the stimulus (Gauriau and Bernard, 2002).

In addition to the afferent flow of pain information, there is also an efferent flow of pain modulating signals (Millan 2002). Structures such as the periaqueductal gray (PAG) and the rostral ventromedial medulla (RVM) project from the brainstem caudally to the spinal cord, where they exert modulatory influence upon the previously described afferent circuitry. These top-down modulatory circuits can adjust the perception of nociceptive stimuli in a pro-nociceptive or anti-nociceptive manner.

Nociplasticity and modeling nociplastic pain

Changes in the neural circuitry underlying pain sensation can drive pain in the absence of tissue injury, a debilitating condition referred to as nociplastic pain (Fitzcharles et al., 2021; Nijs et al 2021). While nociplastic pain can occur independently, it often presents as part of a mixed-pain pathophysiology, arising in parallel with chronic nociceptive or neuropathic pain (Fitzcharles et al., 2021; Kosek et al., 2021; Nijs et al 2021; Maixner et al., 2016). This suggests that persistent pain experience can drive changes in pain perception and produce a generalized pain state. A nociplastic component is estimated to be present in 25% to 75% of chronic pain cases (Dydyk et al., 2023; Fitzcharles et al., 2021). The neural circuitry and neuroplasticity underlying nociplastic pain are not well understood. Interrogating the pathophysiology of this widespread condition is necessary to develop therapeutic interventions that target the mechanistic underpinnings of nociplastic pain, not just the presenting symptoms.

There is currently no broadly accepted model of nociplastic pain. Chronic activation of *Tph2*- expressing neurons in the RVM and *Slc17a6*-expressing neurons in the PBN both produce a long-lasting painful state (Sun et al., 2020; Chen et al., 2017). The neural circuitry underlying this nociplastic effect is not currently understood. Identifying the key

components responsible for driving nociplasticity within this circuit may provide insight into the pathophysiology of chronic nociplastic pain. As such, this thesis uses the artificial activation of neurons within the CNS to model nociplastic pain.

The lateral parabrachial nucleus and *Calca* neurons

Nociceptive signaling from the spinal cord, trigeminal and vagal nerves, and area postrema can activate PBN neurons (Choi et al., 2020; Rodriguez et al., 2017; Hermann et al., 1985; Zhang et al., 2021), which relay those signals to multiple forebrain regions (Pauli et al., 2022; Huang et al., 2021; Chiang et al., 2020; Grady et al., 2020; Saper et al., 1980; Gauriau and Bernard, 2002). The PBN is composed of approximately a dozen molecularly defined glutamatergic neuron subtypes and a minor population of GABAergic neurons (Pauli et al. 2022). Non-specific activation of the PBN glutamatergic neurons can elicit painful phenotypes such as allodynia, while inhibition of those neurons or activation of the GABAergic neurons can inhibit painful phenotypes (Torres-Rodriguez et al., 2023; Zhou et al., 2023; Sun et al., 2020; Chiang et al., 2019). The roles that molecularly defined subsets of PBN neurons contribute to pain sensation is also being explored. For example, chemogenetic activation of PBN *Tac1*-expressing neurons elicits escape-like behaviors (Arthurs, et al. 2023; Barik et al., 2018), whereas chemogenetic or optogenetic activation of *Tacr1*-expressing neurons elicits coping responses to painful stimuli (Barik et al., 2021; Huang et al., 2021; Ma 2021; Deng, et. al., 2020). We and others have shown that PBN *Calca* neurons are activated by aversive stimuli spanning several modalities including some that are considered painful, e.g., foot shock, tail pinch, and formalin- or Freund's adjuvant-induced inflammation (Kang et al., 2022; Campos et al., 2018; Chen et al., 2018; Campos et al. 2017; Han et al., 2015).

Chemogenetic activation of *Calca* neurons promotes anorexia, adipsia, and escape-like behaviors (Arthurs et al., 2023; Carter et al., 2013) whereas more robust stimulation with optogenetics can induce freezing, bradycardia, and fear-like behaviors (Bowen et al., 2020; Han et al., 2015). Most assays have examined the effects of transient activation, but chronic activation can promote severe anorexia (Carter et al., 2013) and the neurological effects of cancer cachexia have been shown to depend on activation of PBN *Calca* neurons (Campos et al., 2017). However, the effects of chronic activation of *Calca* neurons on pain-related phenotypes have not been examined. I hypothesized that activation of *Calca* neurons is necessary to establish allodynia after nerve ligation and that chronic activation of these neurons is sufficient to instate chronic nociplastic pain.

Results

I. Parabrachial *Calca* neurons are necessary for the manifestation of neuropathic pain

Neuropathic pain activates parabrachial *Calca* neurons and drives persistent changes in their excitability

Chronic pain was modeled using unilateral, partial sciatic nerve ligation (pSNL) (Malmberg and Basbaum, 1998) and the presence of neuropathic allodynia was confirmed using the von Frey tactile-sensitivity assay. pSNL produced a significant reduction in the paw-withdrawal threshold both ipsilateral and contralateral to the site of nerve injury (Fig. S1A), consistent with previous findings of bilateral tactile hypersensitivity after nerve injury (Abraham et al., 2020; Raver et al., 2020; Arguis et al., 2008; Koltzenburg et al., 1999). PBN *Calca* neurons are known to act as a primary relay for brief pain signals (Campos et al., 2018; Palmiter, 2018; Han et al., 2015); however, it was not known whether they are involved in the experience of chronic pain. To determine whether they are activated in chronic pain we performed RNAscope *in situ* hybridization on sham or pSNL-operated mice using probes for *Calca, Cck* and the immediate early gene *Fos*, a proxy for neuronal activity (Chung, 2015) (Fig, 1A). We included *Cck* because it was shown to be reduced 30 days following pSNL (Fu et al., 2022) and could serve as a positive control. Three days following pSNL, we observed a significant increase in the colocalization of *Fos* and *Calca* mRNA in the PBN of pSNL-treated animals; however, this effect did not persist at 30 days post-surgery (dps) (Fig. 1B, F). There was no difference in the colocalization of *Calca* and *Fos* at either time

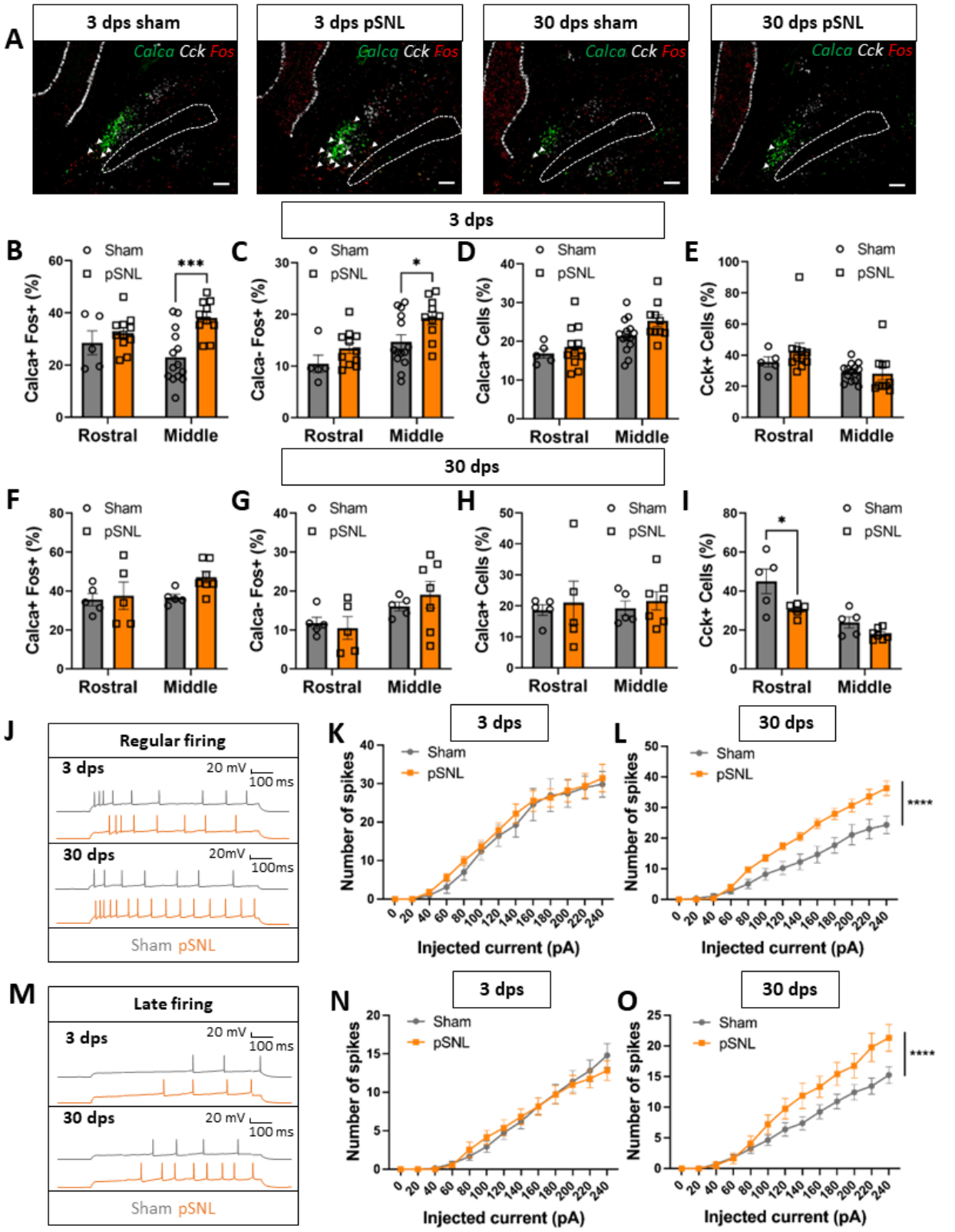

Legend on next page

Figure 1. Neuropathic pain activates parabrachial *Calca* neurons and drives persistent changes in their excitability

(A) Representative images from RNAscope *in situ* hybridization on tissue slices collected 3 or 30 days post sham or pSNL surgery with probes targeting *Calca* (green), *Fos* (red), and *Cck* (white). Scale bar = 100 µm, dotted line marks the superior cerebellar peduncle (SCP), anterior-posterior Bregma level = -5.1.
(B) pSNL increased *Fos* mRNA in *Calca* neurons in the middle, but not the rostral, PBN at 3 dps.
(C) pSNL increased *Fos* mRNA in non-*Calca* neurons in the middle, but not the rostral, PBN at 3 dps.
(D) pSNL did not change the number of *Calca*-positive neurons in the rostral or middle PBN at 3 dps.
(E) pSNL did not change the number of *Cck* positive cells in the rostral or middle PBN at 3 dps.
(B-E) Rostral sham n = 5, middle sham n = 14, rostral pSNL n = 11, and middle pSNL n = 10.
(F) pSNL did not drive an increase in the expression of *Fos* mRNA in *Calca* neurons at 30 dps.
(G) pSNL did not drive an increase in the expression of *Fos* mRNA in non-*Calca* neurons at 30 dps.
(H) pSNL did not change the number of *Calca* positive neurons in the rostral or middle PBN at 30 dps.
(I) pSNL decreased the number of *Cck* positive neurons in the rostral, but not the middle, PBN at 30 dps.
(F-I) Rostral sham n = 5, middle sham n = 5, rostral pSNL n = 5, and middle pSNL n = 7.
(B-I) Significance tested by ANOVA with multiple comparisons. * = $P < 0.05$, *** = $P < 0.001$. Error bars = SEM.
(J) Representative traces showing regular-firing *Calca* neurons 3 and 30 days post sham or pSNL surgery.
(K) pSNL 3 days prior to electrophysiology did not change the number of spikes elicited by current injection in the regular-firing population. Sham n = 3 animals, 7 neurons; pSNL treated n = 3 animals, 13 neurons.
(L) pSNL 30 days prior to electrophysiology increased the number of spikes elicited by current injection in the regular-firing population. Sham n = 4 animals, 9 neurons; pSNL treated n = 4 animals, 9 neurons.
(K-L) 3 dps sham and pSNL biological replicate n = 3. 3 dps sham technical replicate n = 7 and pSNL technical replicate n = 13. 30 dps sham and pSNL biological replicate n = 4. 30 dps sham technical replicate n = 9 and pSNL technical replicate n = 9. Significance measured by ANOVA, **** = $P < 0.0001$. Error bars = SEM.
(M) Representative traces showing late-firing *Calca* neurons 3 and 30 days post sham or pSNL surgery.
(N) pSNL 3 days prior to electrophysiology did not change the number of spikes elicited by current injection in the late-firing population. Sham n = 3 animals, 15 neurons; pSNL treated n = 3 animals, 13 neurons.
(O) pSNL 30 days prior to electrophysiology increased the number of spikes elicited by current injection in the late-firing population. Sham n = 4 animals, 20 neurons; pSNL treated n = 4 animals, 9 neurons.
(N-O) 3 dps sham and pSNL biological replicate n = 3. 3 dps sham technical replicate n = 15 and pSNL technical replicate n = 13. 30 dps sham and pSNL biological replicate n = 4. 30 dps sham technical replicate n = 20 and pSNL technical replicate n = 9. Significance measured by ANOVA, **** = $P < 0.0001$. Error Bars = SEM.

point when comparing the ipsilateral and contralateral PBN, or when comparing males and females (Fig. S1B, C). Additionally, there was a significant increase in the *Fos* induction of *Calca*-negative PBN neurons at 3 dps, but not 30 dps (Fig. 1C, G). There was no change in the expression level of *Calca* within the PBN when comparing sham and pSNL-treated animals at either time point (Fig. 1D, H). However, the percentage of *Cck*-positive neurons was significantly decreased at 30 dps (Fig. 1E, I), consistent with a previous finding (Fu et al., 2022). These data suggest that *Calca* neurons are activated by pSNL. The lack of *Fos* induction in *Calca* neurons at 30 dps does not necessarily mean the pSNL-driven *Calca* neuron activity has waned, as *Fos* induction is a poor marker of chronic changes in neuronal activity (Nestler et al., 2001).

To determine if the excitability of *Calca* neurons changes following pSNL, we performed patch-clamp electrophysiology. Brain slices from *Calca*^{tdTomato} mice that included the PBN were prepared at 3 and 30 dps and the *Calca* neurons were injected with 800-ms pulses of current ranging from 0 to 240 pA. Quantification of the elicited spikes revealed two distinct response patterns, regular and late firing (Fig. 1J, M). No change in excitability was observed in the 3 dps neurons relative to neurons from sham-operated animals (Fig. 1K, N); however, both the regular- and late-firing populations were significantly more responsive to current injection at 30 dps relative to neurons from sham-operated animals (Fig. 1L, O). Taken together, the *in situ* hybridization data and the electrophysiological data reveal that *Calca* neurons are activated by pSNL and this activity increases the intrinsic excitability of *Calca* neurons over time.

Parabrachial *Calca* neurons are necessary for the induction of neuropathic pain

Inhibition of PBN neurons is known to prevent the manifestation of neuropathic injury-driven allodynia (Zhou et al., 2023; Raver et al., 2020; Sun et al., 2020); however, this phenomenon has never been associated with molecularly defined neurons within the PBN. The PBN *Calca* neurons were an attractive candidate because they are activated by pSNL and many other aversive stimuli (Kang et al., 2022; Campos et al., 2018; Palmiter, 2018). To assess the necessity of *Calca* neurons in the manifestation pSNL-driven chronic pain, we injected an AAV expressing Cre-dependent tetanus toxin light chain (AAV-DIO-GFP:TeTx) bilaterally into the PBN of *Calca*$^{Cre/+}$ mice (Fig. 2A) before performing pSNL or sham surgeries. TeTx degrades synaptobrevin, part of the cellular machinery responsible for vesicle release, thus preventing signaling to post-synaptic cells (Kim et al., 2009; Schiavo et al., 2000). Prior to pSNL, a baseline sensitivity to the von Frey (mechanical allodynia) assay was obtained. TeTx expression did not affect baseline paw-withdrawal threshold relative to control animals injected with an AAV expressing Cre-dependent YFP; however, after pSNL, animals treated with TeTx did not develop tactile allodynia (Fig. 2B). Control animals developed allodynia as expected (Fig. 2B). These data suggest that *Calca* neurons are necessary for the manifestation of allodynia in this neuropathic-pain model.

We then asked whether there was a critical window following neuropathic injury during which the activity of *Calca* neurons is necessary for the manifestation of allodynia. We first bilaterally expressed Cre-dependent hM4Di (AAV-DIO-hM4Di:YFP), an inhibitory designer receptor activated by clozapine-N-oxide (CNO) ligand, in the PBN of *Calca*$^{Cre/+}$ mice (Fig. 2C). Tactile sensitivity was assessed at baseline using the von

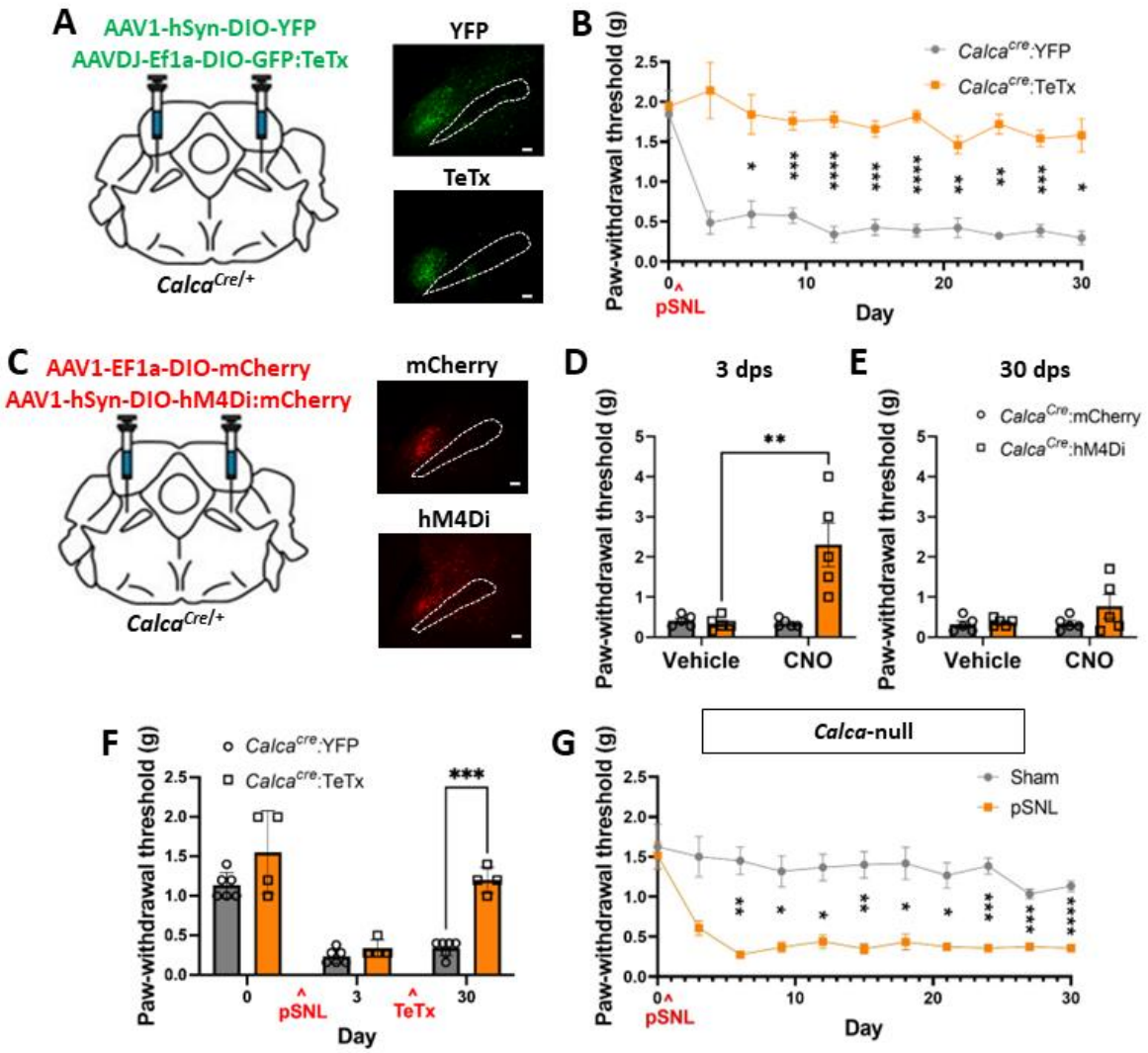

Figure 2. Parabrachial *Calca* neurons are necessary for the induction of neuropathic pain

(A) Bilateral injections of AAV1-hSYN-DIO-YFP or AAVDJ-Ef1a-DIO-GFP:TeTx into the PBN of *Calca*$^{Cre/+}$ mice. Representative images show expression of YFP and TeTx. Scale bar = 100 µm, dotted line marks the SCP, anterior-posterior Bregma level = -5.1.
(B) TeTx expression in PBN *Calca* neurons prevents the development of pSNL driven allodynia measured by von Frey assay. *Calca*$^{Cre/+}$:YFP n = 5 and *Calca*$^{Cre/+}$:TeTx n = 5.
(C) Bilateral injections of AAV1-SYN-DIO-mCherry or AAV1-CBA-DIO-hM4Di:mCherry into the PBN of *Calca*$^{Cre/+}$ mice. Representative images show expression of mCherry and hM4Di:mCherry. Scale bar = 100 µm, dotted line marks the SCP, anterior-posterior Bregma level = -5.1.
(D) hM4Di/CNO inhibition of PBN *Calca* neurons ameliorates pSNL driven allodynia at the 3 dps, measured by von Frey assay. *Calca*$^{Cre/+}$:mCherry n = 5 and *Calca*$^{Cre/+}$:hM4Di n = 5.

Legend continues on next page

(E) hM4Di/CNO inhibition of PBN *Calca* neurons ameliorates pSNL driven allodynia at the 30 dps, measured by von Frey assay. *Calca*$^{Cre/+}$:mCherry n = 5 and *Calca*$^{Cre/+}$:hM4Di n = 5.
(F) Bilateral injections of AAV1-hSYN-DIO-YFP or AAVDJ-Ef1a-DIO-GFP:TeTx into the PBN of *Calca*$^{Cre/+}$ mice 14 days after pSNL ameliorated established allodynia measured by von Frey assay. *Calca*$^{Cre/+}$:YFP n = 6 and *Calca*$^{Cre/+}$:TeTx n = 4.
(G) pSNL produced allodynia in *Calca*-null mice measured by von Frey assay.
(B,D-G) Significance tested by ANOVA with multiple comparisons. * = P < 0.05, ** = P < 0.01, *** = P < 0.001, **** = P < 0.0001. Error bars = SEM.

Frey assay; then all animals received unilateral pSNL. The same assay was repeated at 3 dps first following saline injection (0.9%, i.p.), then following CNO injection (5 mg/kg, i.p.). This sequence was performed again at 30 dps. Three days following pSNL, all the mice developed tactile allodynia, CNO-mediated inhibition of *Calca* neurons returned paw-withdrawal thresholds to baseline levels (Fig. 2D). At 30 dps, the allodynia was still apparent, but readministering CNO did not ameliorate pSNL-driven allodynia (Fig. 2E). After observing that this transient inhibition of *Calca* neurons became ineffective at 30 dps, we explored whether chronically silencing *Calca* neurons would impact established allodynia. This was accomplished by bilaterally injecting virally expressed Cre-dependent TeTx into the PBN of *Calca*$^{Cre/+}$ animals 14 days after inducing allodynia via pSNL. At 3 dps, allodynia was present and it persisted at 30 dps in the control mice (Fig. 2F). However, at 30 dps, the paw-withdrawal threshold of TeTx-treated animals had returned to the normal range (Fig. 2F). Given that transient inhibition of *Calca* neurons did not ameliorate chronically established allodynia, but chronic silencing of *Calca* neurons did, it is likely that neuroplasticity occurs downstream of *Calca* neurons and that the activity of *Calca* neurons is necessary for the maintenance of this downstream pro-nociceptive neuroplasticity.

After observing that activation of PBN *Calca* neurons is necessary for the manifestation of chronic pain following neuropathic injury, we explored whether neuropeptide expression from the *Calca* gene is necessary for the development of allodynia following pSNL. For these experiments, we used homozygous *Calca*$^{Cre/Cre}$ mice because homozygosity precludes expression of calcitonin gene-related protein, CGRP (Allen et al., 2023; Chen et al., 2018). pSNL-induced nerve injury in *Calca*$^{Cre/Cre}$ mice still

produced persistent allodynia (Fig. 2G). In line with previous findings demonstrating that the *Calca* gene is dispensable for acute pain sensation (Zajdel et al., 2021), these data indicate that CGRP is not necessary to drive allodynia in this neuropathic pain model. However, it is worth noting that loss of CGRP alleviates pain in arthritis-, formalin-, and bladder-pain models (Allen et al., 2023; Shinohara et al., 2017; Han et al., 2005).

Discussion

We demonstrated that unilateral pSNL induces chronic bilateral allodynia. Unilateral injury driving bilateral allodynia has been observed in several models of neuropathy (Abraham et al., 2020; Raver et al., 2020; Arguis et al., 2008; Koltzenburg et al., 1999). The bilateral allodynia we observe is consistent with the phenomenon of nociplastic pain, as the allodynia contralateral to the site of injury is mediated by changes within the central nervous system (Fitzcharles et al., 2021). This effect is also consistent with the human experience of nociplastic pain, where nociplastic pain is a frequent component of a mixed pain pathophysiology that arises following nociceptive or neuropathic injury (Fitzcharles et al., 2021). As such, we suspect pSNL can be used to model nociplastic pain.

In situ hybridization revealed that *Calca* neurons are activated acutely following pSNL, indicating that *Calca* neurons play a role in the experience of chronic neuropathic pain. pSNL also resulted in an increase in the intrinsic excitability of *Calca* neurons. These findings suggest that *Calca* neurons are activated by neuropathic pain and that neuropathic pain drives nociplasticity in *Calca* neurons. Chronic silencing of *Calca* neurons via tetanus toxin prevented the development of pSNL-driven allodynia, demonstrating that *Calca* neurons are necessary for the manifestation of chronic

neuropathic pain. Additionally, chronically silencing *Calca* neurons after neuropathic pain was established ameliorated pSNL-driven allodynia, suggesting that *Calca* neurons are also necessary for the maintenance of neuropathic pain. However, transient inhibition of *Calca* neurons did not ameliorate pSNL-driven allodynia. Collectively, these data support the idea that parabrachial *Calca* neurons are activated by chronic neuropathic pain and that this activity results in nociplasticity within Calca neurons, but pronociceptive neuroplasticity likely also occurs downstream.

Supplemental Figures

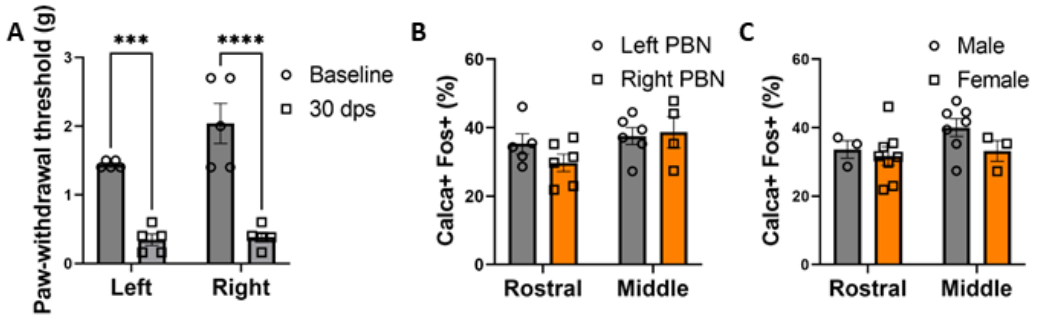

Figure S1. PBN *Calca* neurons bilaterally exhibit uniform activity and do not have sexual dimorphic activity. (Related to Figure 1)

(A) pSNL resulted in bilateral allodynia, n = 5.
(B) There was no difference between left and right PBN *Calca* and *Fos* colocalization 3 days post unilateral (left) pSNL. Rostral left PBN, n = 5; rostral right PBN, n = 6; middle left PBN, n = 6; middle right PBN, n = 4.
(C) There was no difference between male and female PBN *Calca* and *Fos* colocalization 3 days post pSNL. Rostral male, n = 3; rostral female, n = 7; middle male, n = 7; middle female, n = 3.

II. Parabrachial *Calca* neuron activity is sufficient to drive nociplasticity

Chronic activation of *Calca* neurons drives persistent allodynia

Chronic stimulation of all excitatory neurons in the PBN can produce a persistent state of allodynia in the absence of tissue injury (Sun et al., 2020), a nociplastic effect. About 85% of PBN neurons are glutamatergic (Pauli et al., 2023; Karthik et al., 2022), including molecularly defined neurons that mediate different and sometimes opposing behavioral effects (Arthurs et al., 2023; Pauli et al., 2023; Karthik et al., 2022; Bowen et al., 2020; Chiang et al., 2020; Chen et al., 2018; Carter et al., 2013). We repeated the experiment of Sun et al. (2020) by bilaterally injecting AAV carrying a Cre-dependent excitatory receptor activated by CNO, (AAV-DIO-hM3Dq:mCherry) into the PBN of *Slc17a6*$^{Cre/+}$ mice (*Slc17a6* encodes Vglut2, the vesicular glutamate transporter 2). Daily treatment with CNO (1 mg/kg, i.p., 7 days) produced allodynia that developed following the first CNO injection and lasted many days after the last CNO injection, a sign of nociplasticiy (Fig. S2A). We replicated the results of (Sun et al., 2020), who measured mechanical sensitivity 23 h after each CNO injection; however, when von Frey sensitivity was measured 2 h after each CNO injection it produced a remarkable analgesic effect, that dissipated by 23 h revealing allodynia (Fig. S2A, B). The hM3Dq/CNO-driven analgesia in *Slc17a6*$^{Cre/+}$ mice is similar in both scale and transience to the effect of stimulating PBN *Oprm1* neurons, a subset of the greater *Slc17a6* population (Arthurs et al., 2023; Pauli et al., 2023), using the same strategy (Fig. S2C). Consistent with previous studies (Huo et al., 2023), these data show that the PBN *Oprm1* subpopulation can mediate the analgesic effect of stimulating all PBN *Slc17a6* neurons. These findings demonstrate the functional

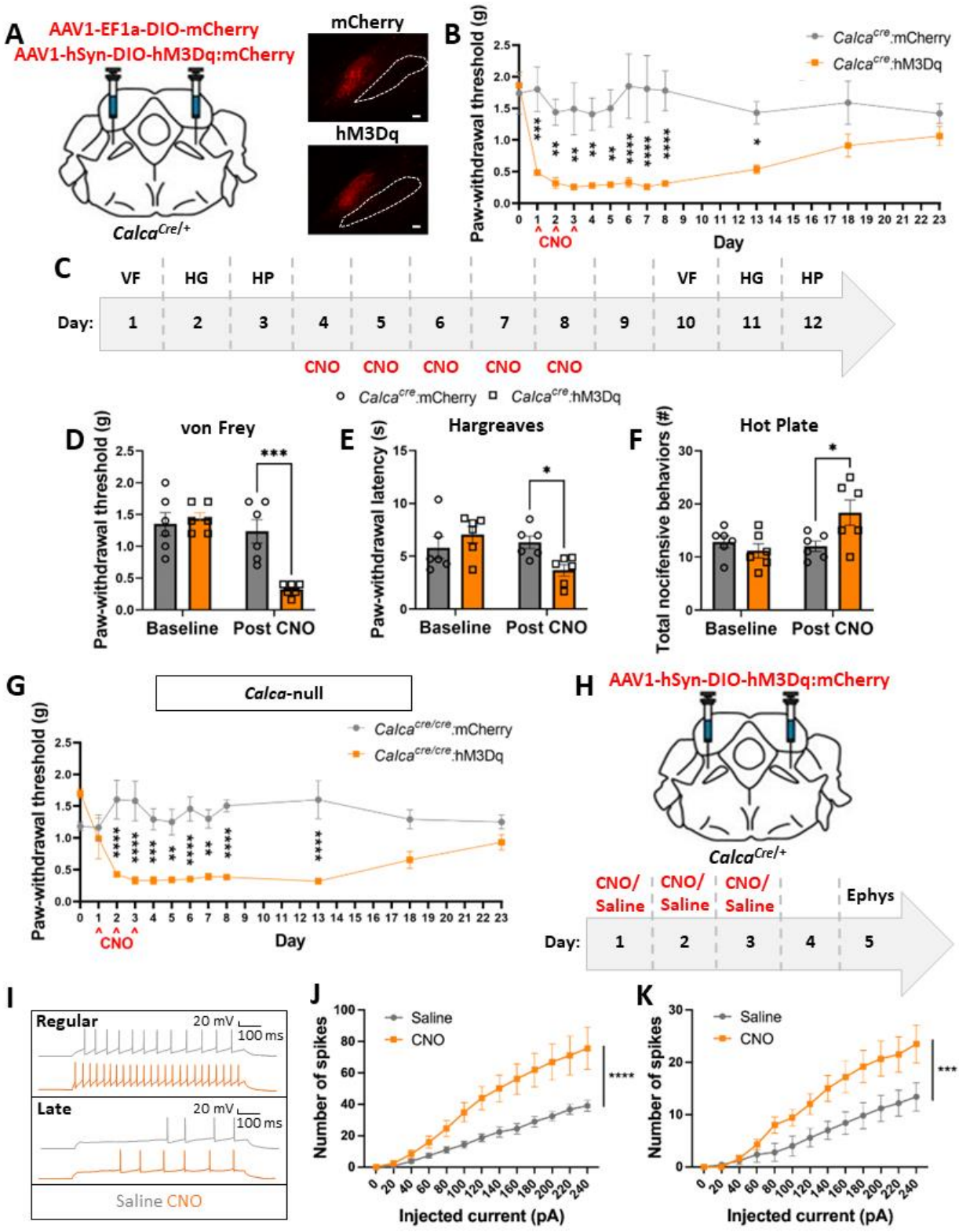

Legend on next page

Figure 3. Activation of parabrachial *Calca* neurons is sufficient to drive nociplasticity

(A) Bilateral injections of AAV1-Ef1a-DIO-mCherry or AAV1-hSyn-DIO-hM3Dq:mCherry into the PBN of *Calca*$^{cre/+}$ mice. Representative images show expression of mCherry and hM3Dq. Scale bar = 100 µm, dotted line marks the SCP, anterior-posterior Bregma level = -5.1.
(B) 3 days of CNO injection (1 mg/kg, i.p.) resulted persistent allodynia measured by von Frey assay. *Calca*$^{cre/+}$:mCherry n = 5 and *Calca*$^{cre/+}$:hM3Dq n = 7.
(C) Behavior timeline for von Frey (VF), Hargreave's (HG), and hot plate (HP) assays before and after 5 consecutive days of CNO injection. *Calca*$^{Cre/+}$:mCherry n = 6 and *Calca*$^{cre/+}$:hM3Dq n = 6.
(D) 5 days of CNO injection decreased paw-withdrawal threshold, measured by von Frey assay, which persists after the last CNO injection.
(E) 5 days of CNO injection decreased in paw-withdrawal latency, measured by Hargreave's assay, which persists after the last CNO injection.
(F) 5 days of CNO injection increases nocifensive behaviors, measured by hot plate assay, which persists after the last CNO injection.
(G) 3 days of CNO injection (1 mg/kg, i.p.) resulted in persistent allodynia measured by von Frey assay. *Calca*$^{Cre/Cre}$:mCherry n = 6 and *Calca*$^{Cre/Cre}$:hM3Dq n = 6.
(B,D-G) Significance tested by ANOVA with multiple comparisons. * = P < 0.05, ** = P < 0.01, *** = P < 0.001, **** = P < 0.0001. Error bars = SEM.
(H) Bilateral injections of AAV1-hSyn-DIO-hM3Dq:mCherry into the PBN of *Calca*$^{cre/+}$ mice followed by 3 days of CNO or saline injection and 48 h of no stimulation prior to electrophysiology.
(I) Representative traces showing regular- and late-firing *Calca* neurons.
(J) 3 days of CNO injection (i.p.) prior to electrophysiology resulted in an increase in the number of spikes elicited by current injection in the regular-firing population. Saline-treated n = 3 animals, 14 neurons; CNO treated n = 3 animals, 11 neurons.
(K) 3 days of CNO injection (i.p.) prior to electrophysiology resulted in an increase in the number of spikes elicited by current injection in the late-firing population. Saline-treated n = 3 animals, 5 neurons; CNO treated n = 3 animals, 11 neurons.
(J-K) Significance measured by ANOVA. *** = P < 0.001, **** = P < 0.0001. Error Bars = SEM.

heterogeneity of excitatory neurons within the PBN and are consistent with the molecular heterogeneity of this brain region (Pauli et al., 2023; Karthik et al., 2022).

Given that PBN *Calca* neurons are necessary for the manifestation of neuropathic injury-driven allodynia, we hypothesized that activation of PBN *Calca* neurons might be sufficient to produce nociplasticity. To test this idea, we injected an AAV carrying Cre-dependent hM3Dq:mCherry (or just mCherry as control) bilaterally into the PBN of *Calca*$^{Cre/+}$ mice (Fig. 3A). After waiting several weeks for viral expression, 3 consecutive days of CNO delivery (1 mg/kg, i.p.) resulted in significant tactile allodynia 2 h and 23 h post injection that persisted for 10 days following the last CNO injection (Fig. 3B, Fig. S2D). We noted a sexually dimorphic effect in the dissipation, but not the development, of allodynia (Fig. S2E). Additionally, unilateral injection of Cre-dependent hM3Dq:mCherry and subsequent treatment with CNO produced bilateral allodynia (Fig. S2F, G). To determine whether this persistent allodynic effect was in fact nociplasticity, not simply a learned association between the von Frey chamber and *Calca*-neuron-driven aversive sensation, we performed a set of pain assays before and after, but not during, 5 days of CNO administration (Fig. 3C). Two days after the last CNO injection, we observed a significant decrease in von Frey paw-withdrawal threshold, Hargreaves paw-withdrawal latency, and the number of nocifensive behaviors performed on a hot plate (Fig. 3D-F). We also tested whether chronic activation of *Calca* neurons alters locomotor ability as well as anxiety and depression-related behaviors (Fig. S3A). After 5 days of CNO or saline administration, CNO-treated animals exhibited elevated locomotor activity in the open-field assay, elevated freezing in the tail-suspension test relative to controls, and decreased paw- withdrawal threshold (Fig. S3B, E, F). There was

a trend towards a significant decrease in sucrose preference ($p = 0.176$, Fig. S3G) and no significant effect in the open-field center time or elevated-plus-maze assays (Fig. S2C, D). The persistent allodynia and hyperalgesia observed in these assays supports our conclusion that chronic activity in the PBN *Calca* population is sufficient to drive nociplasticity.

Given that activation of PBN *Calca* neurons is sufficient to drive nociplastic pain, we asked whether expression of the *Calca* gene is a necessary part of these phenomena. We performed 3 consecutive days of hM3Dq-mediated stimulation of PBN *Calca* neurons in *Calca*$^{Cre/Cre}$ mice. This manipulation produced allodynia that lasted 10 days after CNO cessation (Fig. 3G), like the effect observed using heterozygous *Calca*$^{Cre/+}$ mice (Fig. 3B). These data indicate that, while activation of PBN *Calca* neurons is sufficient to drive nociplasticity, the *Calca* gene products, including CGRP, do not play a necessary role in this model of nociplastic pain.

We have established that *Calca* neuron activity is sufficient to drive nociplasticity; however, the neuronal populations exhibiting neuroplastic changes as a result of this stimulation paradigm are not yet established. We performed patch-clamp electrophysiology to assess the excitability of *Calca* neurons expressing hM3Dq:mCherry following 3 days of either CNO or saline injections (Fig. 3H, I). Forty-eight hours following the final injection, at which point all injected CNO should be metabolized (Raper et al., 2017), *Calca* neurons in slices were injected with 800-ms pulses of current ranging from 0 to 240 pA. Quantification of the elicited spikes once again revealed two distinct response patterns, regular and late firing (Fig. 3J). Both the regular- and late-firing populations were significantly more responsive to current

injection when the mice were pretreated with CNO rather than saline (Fig. 3K, L). These data demonstrate that this direct activation of *Calca* neurons produces a persistent increase in their intrinsic excitability.

Nociplastic effect scales with the duration of *Calca* neuron excitation

Seven days of stimulating *Slc17a6* neurons in the PBN produces persistent (>30 days) nociplasticity (Sun et al., 2020 and Fig. S2A) and three days of stimulating *Calca* neurons in the PBN produces a nociplastic effect that lasted 10 days (Fig. 3B). These findings suggest that nociplasticity scales with the duration of *Calca* neuron stimulation. To further examine this phenomenon, we stimulated PBN *Calca* neurons expressing hM3Dq just once and assessed tactile allodynia until paw withdrawal thresholds returned to baseline. One day of CNO-driven stimulation of *Calca* neurons produced 4 days of allodynia (Fig. 4A, B).

Even more acute activation was achieved by bilateral stimulation of channelrhodopsin (ChR2) that was targeted to the PBN *Calca* neurons. Twenty min of bilateral 473-nm (20 Hz, 10 mW, 2 s “on”, 2 s “off”) light application over the *Calca* cell bodies produced allodynia within an hour and persisted 2 days after stimulus cessation (Fig. 4C, D). Even 5 min of bilateral stimulation produced allodynia that was weaker, but persisted for 2 days (Fig. 4E). Additionally, 5 min of stimulation performed daily for 5 days produced a nociplastic effect that lasted 15 days after the last stimulation (Fig. 4F). A single 20-min unilateral stimulation using the same parameters also produced bilateral nociplasticity (Fig. S4). Together these data suggest that the duration of PBN *Calca* neuron stimulation dictates the duration of the resultant nociplasticity.

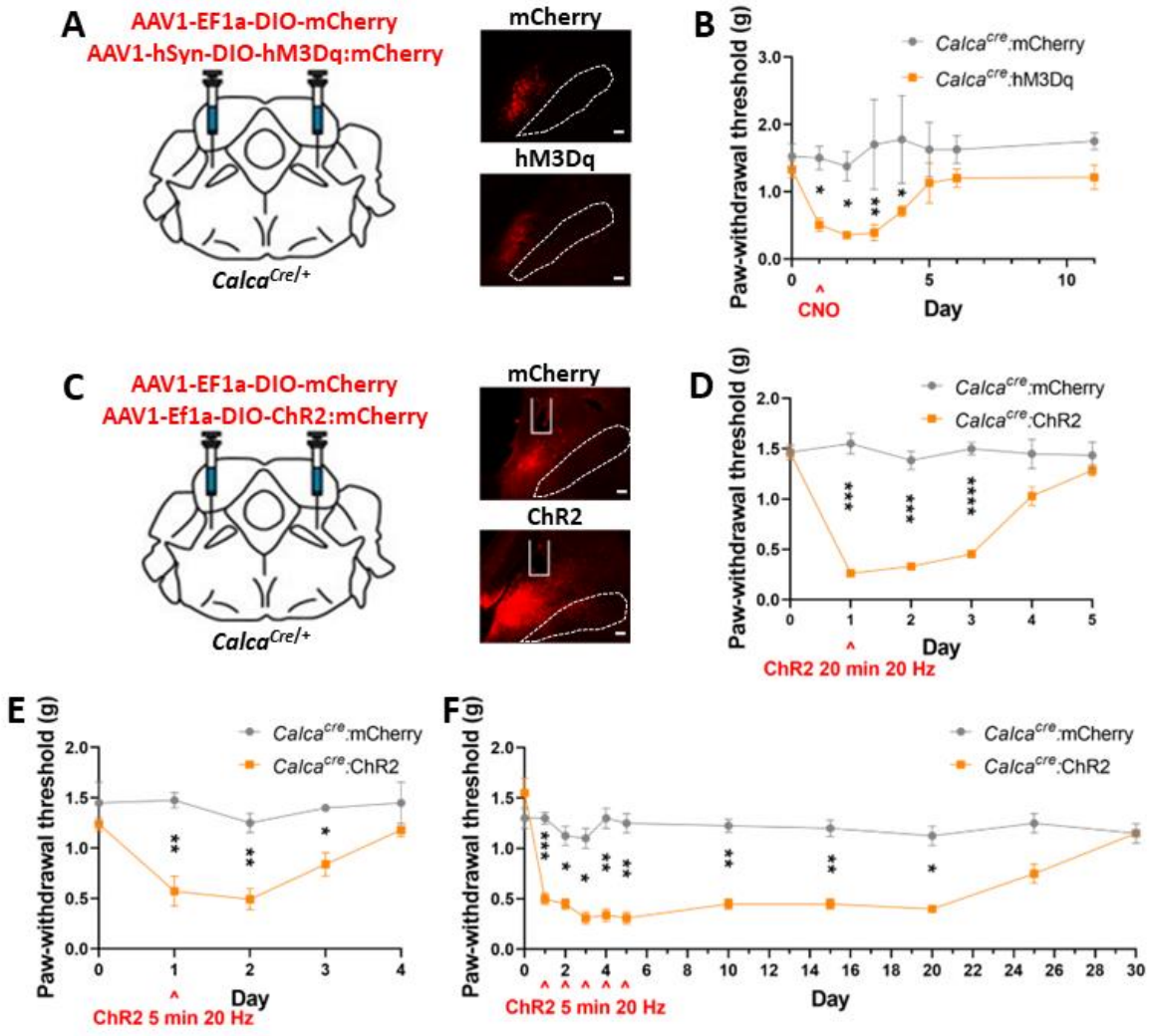

Figure 4. Nociplastic effect scales with the duration of *Calca* neuron activation

(A) Bilateral injections of AAV1-Ef1a-DIO-mCherry or AAV1-hSyn-DIO-hM3Dq:mCherry into the PBN of *Calca*$^{cre/+}$ mice. Representative images show expression of mCherry and hM3Dq. Scale bar = 100 µm, dotted line marks the SCP, anterior-posterior Bregma level = -5.1.
(B) 1 day of CNO injection (1 mg/kg, i.p.) produced allodynia measured by von Frey assay. *Calca*$^{cre/+}$:mCherry n = 4 and *Calca*$^{cre/+}$:hM3Dq n = 7.
(C) Bilateral injections of AAV1-Ef1a-DIO-mCherry or AAV1-Ef1a-DIO-ChR2:mCherry into the PBN of *Calca*$^{cre/+}$ mice. Representative images show expression of mCherry and ChR2. Scale bar = 100 µm, dotted line marks the SCP, anterior-posterior Bregma level = -5.1..
(D) 20 min of 473-nm photostimulation (20 Hz, 2 s on 2 s off) resulted in allodynia measured by von Frey assay. *Calca*$^{cre/+}$:mCherry n = 6 and *Calca*$^{cre/+}$:ChR2 n = 7.

Legend continues on next page

(E) 5 min of 473-nm photostimulation (20 Hz, 2 s on 2 s off) resulted in allodynia measured by von Frey assay. *Calca*$^{cre/+}$:mCherry n = 4 and *Calca*$^{cre/+}$:ChR2 n = 5.
(F) 5 days of 5-min, 473-nm photostimulation (20 Hz, 2 s on 2 s off) resulted in allodynia measured by von Frey assay. *Calca*$^{cre/+}$:mCherry n = 4 and *Calca*$^{cre/+}$:ChR2 n = 4.
(B,D-F) Significance tested by ANOVA with multiple comparisons. * = P < 0.05, ** = P < 0.01, *** = P < 0.001, **** = P < 0.0001. Error bars = SEM.

Chronic exposure to aversive stimuli drives nociplasticity

PBN *Calca* neurons respond to aversive stimuli spanning a range of sensory modalities (Kang et al., 2022; Campos et al., 2018; Chen et al., 2018; Campos et al., 2016; Han et al., 2015). Given that stimulation of *Calca* neurons is sufficient to drive nociplasticity, we explored whether the induction of nociplasticity was agnostic to stimulus modality. Cisplatin chemotherapy (Alhadeff et al., 2017; Park et al., 2013; Ta et al., 2009), lithium chloride (LiCl)-induced visceral malaise (Chen et al., 2018; Carter et al., 2015), foot shock (Campos et al., 2018), and the threat of predation (Kang et al., 2022) have all be demonstrated to activate PBN *Calca* neurons. Chronic exposure to cisplatin (Park et al., 2013), nitroglycerin (NTG; a model for migraine pain) (Pradhan et al., 2014), and foot shock (Wu et al., 2020) are known to produce persistent allodynia. Consistent with previous studies (Pradhan et al., 2014), we found that 5 days of NTG exposure (10 mg/kg, i.p.) produced persistent allodynia (Fig. 5A). We also found that 3 days of injection with LiCl (0.2 M at 15 mL/kg, i.p.) produced persistent allodynia (Fig. 5B). Even 3 days of exposure to a predatory threat (5-min chase daily for 3 days with a toy robotic bug) could promote mild nociplasticity, measured by von Frey assay (Fig. 5C).

NTG- and cisplatin-produced nociplasticity were prevented by prior expression of TeTx in *Calca* neurons (Fig. 5D, E, F). Interestingly, the photophobia that developed following NTG injection did not persist as long as the allodynia (Fig. S5A). Additionally, despite pretreatment of the PBN *Calca* neurons with TeTx, photophobia still occurred following NTG injection (Fig. S5B). These data suggest that chronic exposure to these aversive stimuli, spanning a range of sensory modalities, can induce nociplasticity via the activation of *Calca* neurons.

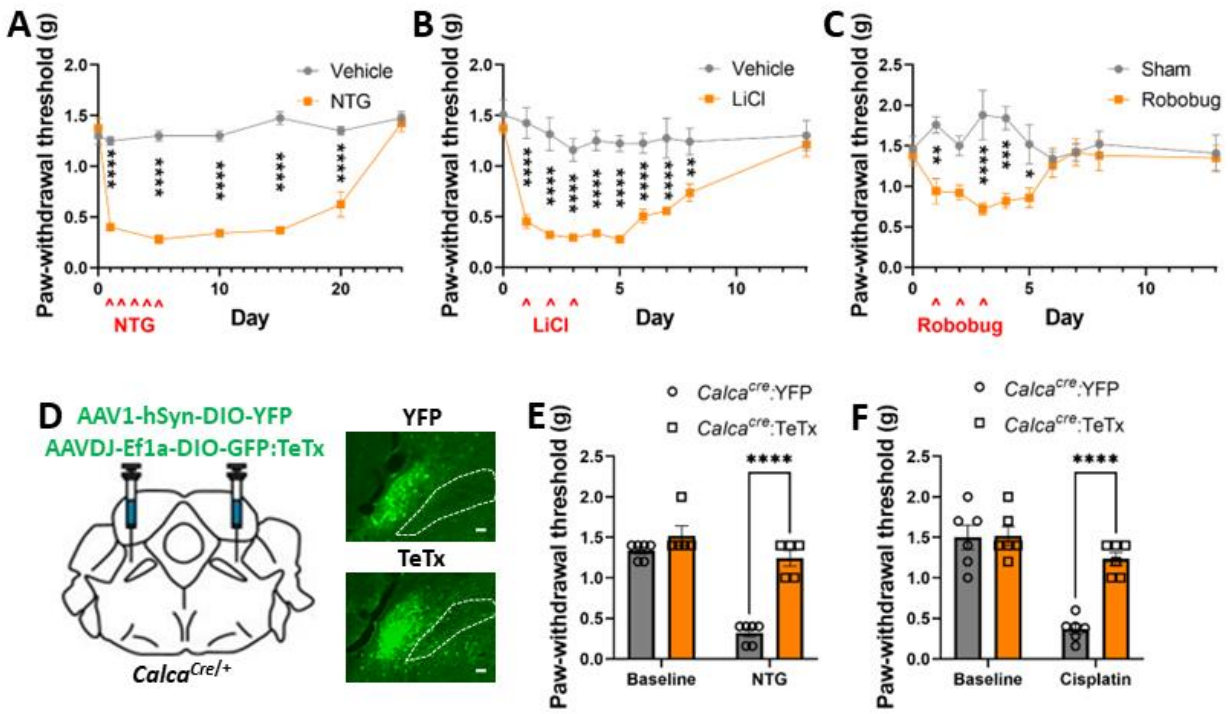

Figure 5. Chronic exposure to all aversive stimuli tested drives nociplasticity regardless of sensory modality

(A) 5 days of NTG exposure (10 mg/kg, i.p.) produced allodynia measured by von Frey assay. Vehicle n = 4 and NTG n = 4.
(B) 3 days of LiCl exposure (0.2 M, 15 mL/kg, i.p.) produced allodynia measured by von Frey assay. Vehicle n = 6 and LiCl n = 8.
(C) 3 days of robobug chase (10 min) produced allodynia measured by von Frey assay. Vehicle n = 5 and robobug n = 5.
(D) Bilateral injections of AAV1-hSYN-DIO-YFP or AAVDJ-Ef1a-DIO-GFP:TeTx into the PBN of *Calca*$^{Cre/+}$ mice. Representative images show expression of YFP and TeTx. Scale bar = 100 µm, dotted line marks the SCP, anterior-posterior Bregma level = -5.1.
(E) TeTx expression in PBN *Calca* neurons prevented the development of NTG-driven allodynia measured by von Frey assay. *Calca*$^{Cre/+}$:YFP n = 6 and *Calca*$^{Cre/+}$:TeTx n = 5.
(F) TeTx expression in PBN *Calca* neurons prevented the development of cisplatin-driven allodynia measured by von Frey assay. *Calca*$^{Cre/+}$:YFP n = 6 and *Calca*$^{Cre/+}$:TeTx n = 6.
(A-C,E-F) Significance tested by ANOVA with multiple comparisons. * = P < 0.05, ** = P < 0.01, *** = P < 0.001, **** = P < 0.0001. Error bars = SEM.

Discussion

We demonstrate that daily chemogenetic or optogenetic stimulation of *Calca* neurons is sufficient to induce allodynia and hyperalgesia that persists for many days beyond the stimulation period. These chronic pain symptoms are the result of generalized nociplasticity and not a learned association between the assays and the aversion generated by *Calca* neuron activity. Additionally, daily chemogenetic stimulation of *Calca* neurons resulted in an increase in the intrinsic excitability of *Calca* neurons similar to that observed 30 days following pSNL. Although *Calca* neuron activity is both necessary and sufficient to generate chronic pain, *Calca* gene products (i.e., CGRP) themselves did not play a significant role in this effect, which is unexpected because CGRP signaling is important in other pain models (Allen et al., 2023; Shinohara et al., 2017; Han et al., 2015).

Sun et al., (2020) reported that 7 days of chemogenetic activation of all glutamatergic neurons in the PBN could produce allodynia that lasted for many days after the final CNO injection. We obtained similar results when assaying von Frey sensitivity 23 h after each CNO injection, when CNO would have been cleared from the circulation. Remarkably, when we assayed allodynia 2 h after each CNO injection, when hM3Dq would still be activated, there was a dramatic analgesic effect. A similar effect was achieved with hM3Dq-mediated stimulation of *Oprm1* neurons. In contrast, chemogenetic activation *Calca* neurons, which represent ~15% of the glutamatergic neurons (Pauli et al., 2022), drives allodynia at both 2 and 23 h after CNO. This result suggests that the glutamatergic population includes neurons that promote allodynia (*Calca* neurons) and those that promote analgesia (*Oprm1* neurons). Both genes are expressed in several

molecularly defined clusters in the PBN (Pauli et al., 2022). The activation of *Oprm1* neurons is aversive (Liu et al., 2022), so it is likely the analgesia we observed was “stress-induced” (Butler and Finn, 2009).

Calca-neuron-mediated nociplasticity scales with stimulus duration. Multiple rounds of chemogenetic stimulation produced allodynia that persisted longer than a single stimulation. Likewise, a brief optogenetic stimulation produced allodynia that was less persistent than after multiple stimulations. The stimulus scaling of nociplasticity that we observed is consistent with the conclusion that *Calca* neuron activity drives nociplasticty.

Several studies, ours included, have demonstrated that unilateral neuropathic injury can produce bilateral pain (Sugimoto et al., 2021; Abraham et al., 2020; Raver et al., 2020; Arguis et al., 2008; Koltzenberg et al., 1999). This phenomenon indicates that persistent pain can induce generalized nociplasticity. Because artificial activation of *Calca* neurons is sufficient to produce generalized pain and that a wide variety of aversive situations activate *Calca* neurons, some of which are not generally considered to be painful, we predicted that many aversive experiences, especially if repeated, would have the capacity to drive nociplasticity. Chronic exposure to NTG (a model of migraine) was shown to produce persistent allodynia (Pradhan et al., 2014), an effect that we duplicated and went on to show was dependent on activation of *Calca* neurons. Similarly, cisplatin-induced chemotherapy can produce allodynia (Park et al, 2013), activate *Calca* neurons (Ta et al., 2009; Park et al., 2013; Alhadeff et al., 2017) and produce persistent allodynia that we show depends on *Calca*-neuron activation in the PBN. We also demonstrate that prolonged visceral malaise (nausea) induced by treatment with LiCl, as well as predatory simulation are sufficient to induce allodynia that may persist for many days. These

findings point to a mechanism by which diverse and polymodal aversive experiences can produce nociplastic pain phenotypes via the activation of PBN *Calca* neurons. This result implies that nociplastic pain may be produced by adverse life events that are distinct from somatic nerve injury. This phenomenon has been observed epidemiologically. Individuals with adverse childhood experiences are significantly more likely to develop chronic pain (Groenewald et al., 2020; Dokyoung et al., 2019; Sherman et al., 2015). These findings may also explain the high degree of mixed pain pathophysiology in chronic pain patients (Fitzcharles et al., 2021). In this circumstance, persistent nociceptive or neuropathic pain may drive nociplastic pain via the chronic activation of *Calca* neurons.

Supplemental figures

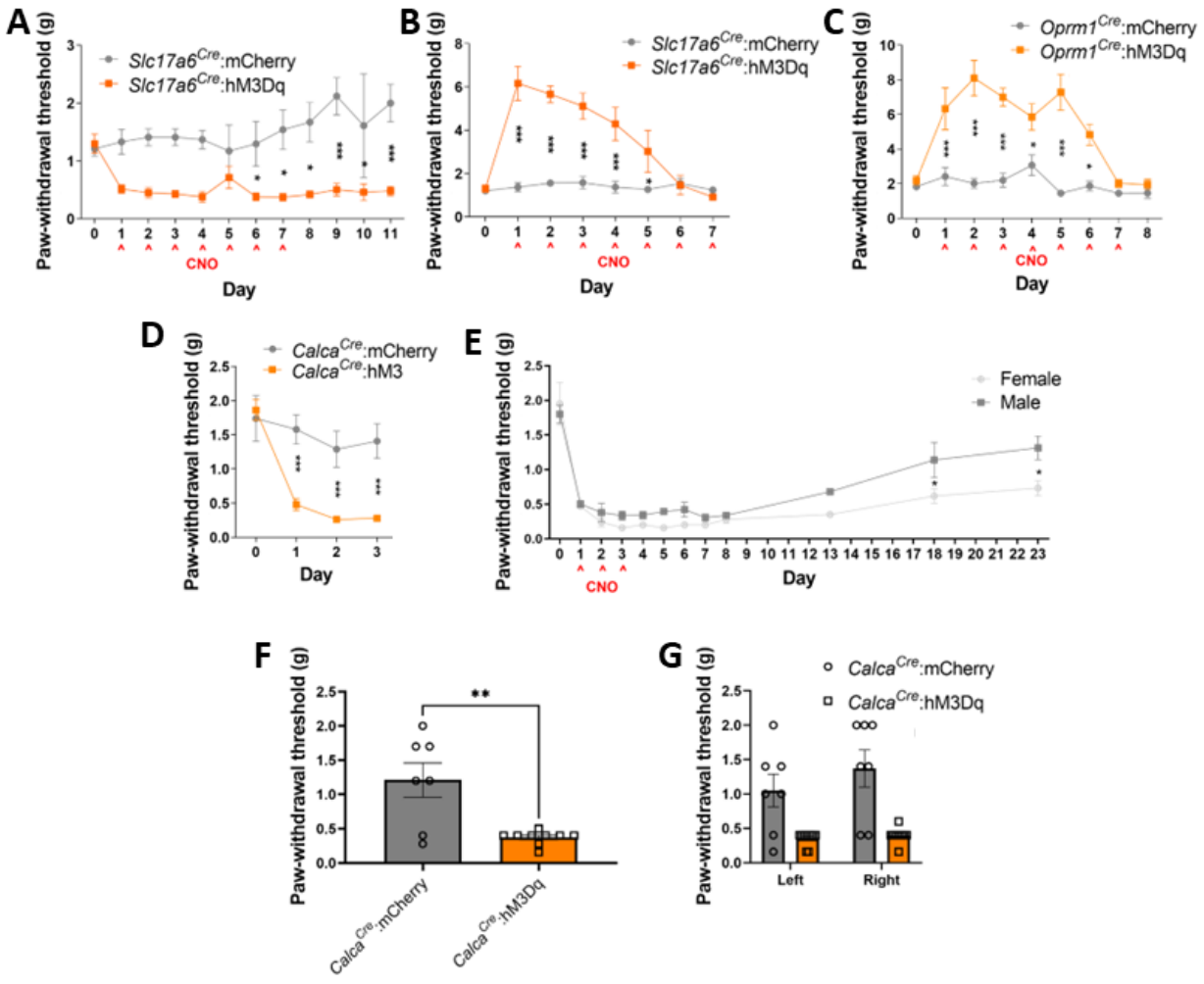

Figure S2. Stimulation of PBN subpopulations (Related to Figure 3)

(A) Chronic stimulation of PBN *Slc17a6* (Vglut 2) neurons via hM3Dq and CNO resulted in persistent allodynia (measured 23 h post injection).
(B) Stimulation of PBN *Slc17a6* neurons via hM3Dq and CNO resulted in analgesia 2 h post injection.
(A-B) *Slc17a6*^{Cre}:mCherry n = 5, *Slc17a6*^{Cre}:hM3Dq n = 6.
(C) Stimulation of PBN *Oprm1* neurons via hM3Dq and CNO resulted in analgesia 2 h post injection. *Oprm1*^{Cre}:mCherry n = 5, *Oprm1*^{Cre}:hM3Dq n = 7.
(D) Stimulation of PBN *Calca* neurons via hM3Dq and CNO resulted in allodynia 23 h after CNO treatment. *Calca*$^{cre/+}$:mCherry n = 5 and *Calca*$^{cre/+}$:hM3Dq n = 7.
(E) Stimulation of PBN *Calca* neurons via hM3Dq and CNO resulted in persistent allodynia in both male and female animals. Female, n = 3; male, n = 4.
(F) Unilateral stimulation of PBN Calca neurons via hM3Dq and one injection of CNO resulted in allodynia measured 2 hr later. *Calca*$^{cre/+}$:mCherry n = 7 and *Calca*$^{cre/+}$:hM3Dq n = 10.
(G) Unilateral stimulation of PBN Calca neurons via hM3Dq and CNO affected left and right hind paw-withdrawal threshold equivalently. *Calca*$^{cre/+}$:mCherry n = 7 and *Calca*$^{cre/+}$:hM3Dq n = 10.

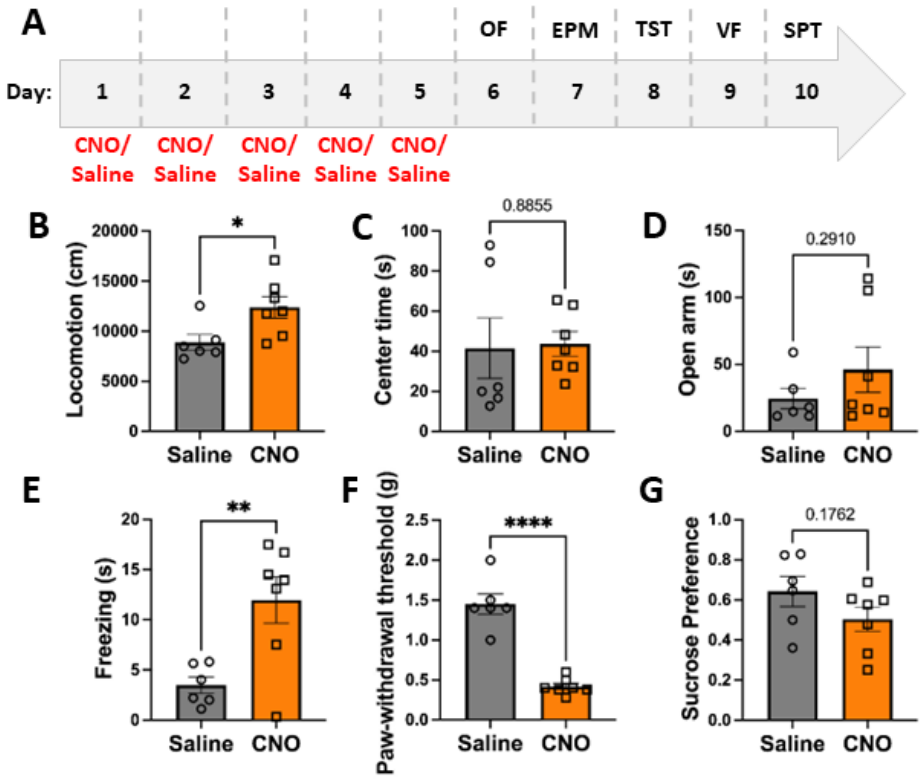

Figure S3. Chronic stimulation of PBN subpopulations (Related to Figure 3)

(A) Behavior timeline for open field (OF), elevated plus maze (EPM), tail-suspension test (TST), von Frey (VF), and sucrose-preference test (SPT) before and after 5 consecutive days of CNO or saline injection. *Calca*$^{Cre/+}$:hM3Dq with i.p. saline n = 6 and *Calca*$^{cre/+}$:hM3Dq with i.p. CNO n = 6.
(B) 5 days of CNO injection increased open field locomotion.
(C) 5 days of CNO injection did not affect time spent in the center of the arena during the open field assaay.
(D) 5 days of CNO injection did not affect time spent in the open arms during the elevated plus maze assay.
(E) 5 days of CNO injection increased time spent freezing during the tail suspension test.
(F) 5 days of CNO injection decreased paw-withdrawal threshold in the von Frey assay.
(G) 5 days of CNO injection did not significantly affect sucrose preference in the sucrose preference test.

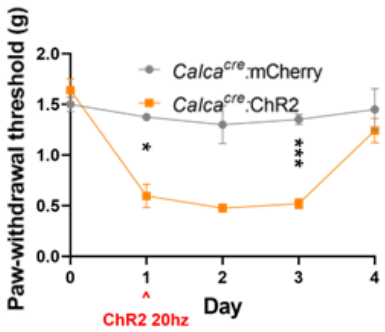

Figure S4. Unilateral optogenetic stimulation of *Calca* neurons (Related to Figure 4)

Unilateral stimulation of PBN *Calca* neurons via ChR2 and 473-nm light (20 min, 20 Hz, 2 s on 2 s off) resulted in persistent allodynia. *Calca*$^{cre/+}$:mCherry n = 4 and *Calca*$^{cre/+}$:ChR2 n = 4.

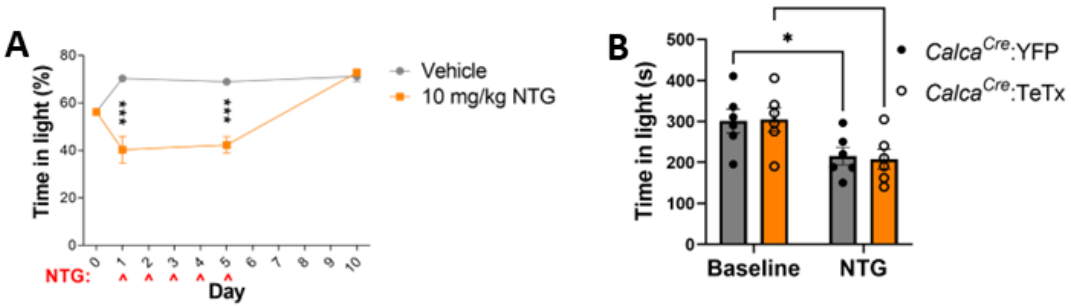

Figure S5. NTG induced photophobia (Related to Figure 5)

(A) NTG injection resulted in photophobia that did not persist past the point of NTG administration. Vehicle, n = 4; NTG, n = 4.
(B) TeTx expression in PBN *Calca* neurons did not prevent the development of NTG-driven photophobia.

Calca$^{Cre/+}$:YFP n = 6 and *Calca*$^{Cre/+}$:TeTx n = 6.

III. *Calca* neurons exhibit plasticity following activation

Robust aversive stimulation changes the population activity of *Calca* neurons

NTG administration induces *Calca*-neuron-dependent, persistent allodynia, like the effect of hM3Dq/CNO mediated stimulation, so we hypothesized it does so by increasing the activity of *Calca* neurons. To investigate this hypothesis, we conducted Ca^{2+} imaging experiments in which we tracked the activity of individual *Calca* neurons across multiple days. To monitor the activity of *Calca* neurons in behaving animals, AAV-DIO-GCaMP6m was expressed, and a Gradient Refractive Index (GRIN) lens was implanted over the PBN of *Calca*$^{Cre/+}$ mice. After 4 weeks of recovery, a microendoscope was attached to each mouse and left in place for 4 consecutive days. This strategy ensured a stable field of view for tracking individual neurons each day. On day 1, mice received an intraperitoneal injection of vehicle and on day 2 they received NTG (10 mg/kg, i.p.). After each injection, mice were placed in the von Frey-testing apparatus for 35 min of acclimation, followed by 5 min of baseline neuronal activity measurement, and then 10 min of von Frey testing (8 filament applications, with a 1-min intertrial interval). On days 3 and 4, *Calca* neurons were imaged again without further injections to determine if NTG treatment had residual effects that could drive persistent allodynia (Fig. 6A).

We tracked the same 79 neurons throughout the experiment (Fig. 6B). NTG administration dramatically increased the basal fluorescence level of most of the *Calca* neurons compared to vehicle administration (Fig. 6B, C). Notably, this elevated fluorescent activity was sustained on the 2 days following NTG injection (Fig. 6B, C); 60% of neurons continued to exhibit elevated basal fluorescence on

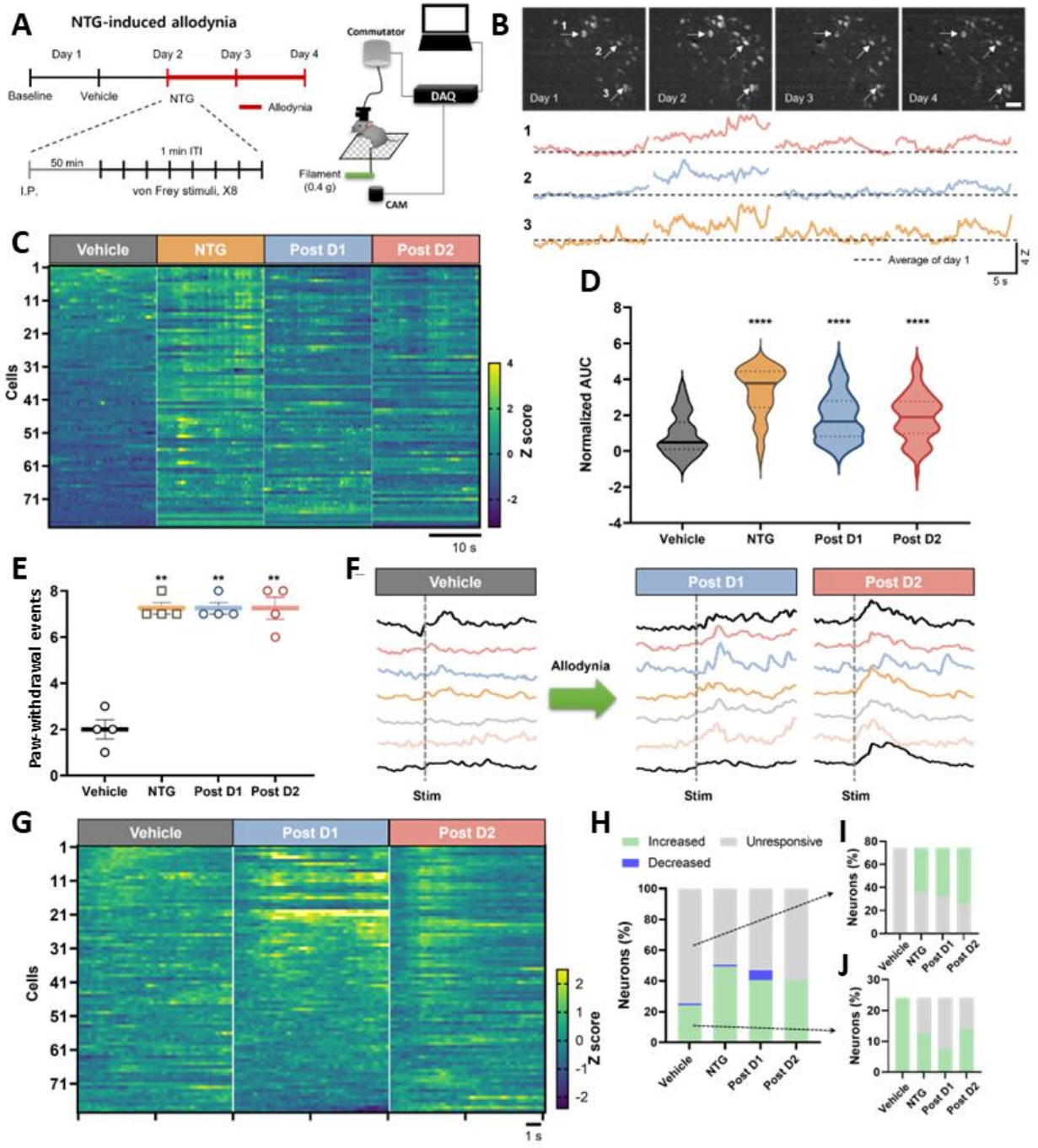

Figure 6. *Calca* neuron activity during the development of mechanical allodynia.

(A) Schematic depiction of Ca2+ imaging during NTG induced mechanical allodynia.
(B) Multi-day tracking of *Calca* neuron fluorescent activity. Top; Field of view (FOV) of representative animal for 4 days. Bottom; representative neural activities throughout 4 days of 3 neurons marked by arrows in FOVs. Scale bar = 50 μm.

Legend continues on next page

(C) NTG injection increased unstimulated neuronal activity. Elevated neuronal activity persisted 24 and 48 h post injection. Individual neurons are aligned across days in heatmap.
(D) Average calcium transient area under the curve increased following NTG injection. This increase in fluorescent activity remained elevated 24 and 48 h post injection.
(E) NTG injection increased the number of times out of 8 applications that mice responded to a 0.4-g von Frey filament. Bar indicates mean ± S.E.M.
(F) Representative traces of filament-evoked neural activities.
(G) The number of *Calca* neurons responsive to application of a 0.4-g von Frey filament increased after NTG injection. The increase in responsive neurons persisted 24 and 48 h after NTG injection.
(H) The percentage of *Calca* neurons responsive to application of a 0.4-g von Frey filament increased from 24% after vehicle injection to 49.5% after NTG injection. The percent of 0.4-g von Frey filament-responsive neurons remained elevated, at 40.5%, 24 and 48 h after NTG injection.
(I) The majority of neurons unresponsive to 0.4-g von Frey filament application following vehicle injection (i.p.) became responsive to the 0.4-g filament following NTG injection (i.p.).
(J) About half of neurons responsive to 0.4-g von Frey filament application following vehicle injection (i.p.) became unresponsive to the 0.4-g filament following NTG injection (i.p.).
(A – J) n = 4 animals, 79 neurons. Significance tested by ANOVA with multiple comparisons. * = $P < 0.05$, ** = $P < 0.01$, *** = $P < 0.001$, **** = $P < 0.0001$. Error bars = SEM.

days 3 and 4 (Fig. 6C, Fig. S6A). The number and amplitude of Ca^{2+} transients did not change across days (Fig. S6B, C). The averaged basal fluorescence level of all 79 neurons (4 mice) increased after NTG administration and remained elevated for two days (Fig. 6D).

We also examined whether NTG administration was accompanied by an increase in the von Frey-elicited responses of individual neurons. NTG injection increased paw-withdrawal responses of all the mice to a low-threshold (0.4 g) von Frey filament (Fig. 6E). Some neurons that exhibited increased activity following von Frey stimuli to vehicle injection showed similar activity after NTG injection (Fig. 6F), while most *Calca* neurons displayed increased fluorescence only after NTG injection (Fig. 6F, G). On the vehicle-injection day, 24% of neurons were activated by the 0.4-g von Frey filament, whereas 49.4% were activated after NTG treatment and 40.5% responded on days 3 and 4. (Fig. 6H). Analysis of individual *Calca* neurons across experimental days revealed that 56.7% of the initially unresponsive neurons became responsive after NTG, with similar values on days 3 and 4 (Fig. 6I). Of the von Frey-responsive neurons on the vehicle-injection day, about half lost their responsiveness following NTG injection and across the subsequent imaging sessions (Fig. 6J). There were no persistent changes in the area under the curve of calcium transients, the number of calcium transients, or the amplitude of calcium transients following 0.4-g von Frey stimulation (Fig. S6D, E, F). These data suggest that the primary effect of NTG treatment is the recruitment of more *Calca*-responsive neurons rather than an increase in the frequency or magnitude of their responses.

Intrathecal injection of neuropeptide Y does not reverse hM3Dq/CNO-driven allodynia

How does manipulation of neurons in the brain result in tactile allodynia allowing gentle touch to appear painful? The allodynia that develops after sciatic nerve injury has been shown to involve plasticity in spinal dorsal horn inhibitory neurons that normally prevent (gate) low-threshold primary afferent (Aß) activity from reaching the nociceptive spinoparabrachial projection neurons, thereby allowing gentle touch to the hind paw to promote paw withdrawal as if it was painful (Cao et al., 2022; Nelson et al., 2022; Peirs et al., 2021; Boyle et al., 2019; Petitjean et al., 2015; Lu et al., 2013; Todd et al., 2010). We hypothesized that chemogenetic activation of *Calca* neurons may activate descending circuits to the spinal cord resulting in plasticity that resembles that induced by nerve injury. Pharmacological or genetic manipulations of several different populations of excitatory neurons in the spinal cord have been shown to reverse peripheral nerve injury-induced allodynia (Cao et al., 2022; Nelson et al., 2022; Peirs et al., 2021). For example, intrathecal injection of the NPY Y1 receptor 1 agonist $NPY^{Leu,Pro}$ has been shown to transiently reduce allodynia after sciatic nerve injury (Nelson et al., 2022, Nelson et al., 2021; Malet et al., 2017). Thus, we tested our hypothesis by intrathecal injection of $NPY^{Leu,Pro}$ into mice with pSNL (as positive control) or mice that had developed tactile allodynia after 3 days of *Calca* neuron activation (Fig. 7A). $NPY^{Leu,Pro}$ injections ameliorated the allodynia produced by pSNL as expected (Fig. 7B) but had no effect on the allodynia that developed after *Calca* neuron activation (Fig. 7C), indicating that the nociplastic allodynia that develops after *Calca* neuron activation does not rely on the

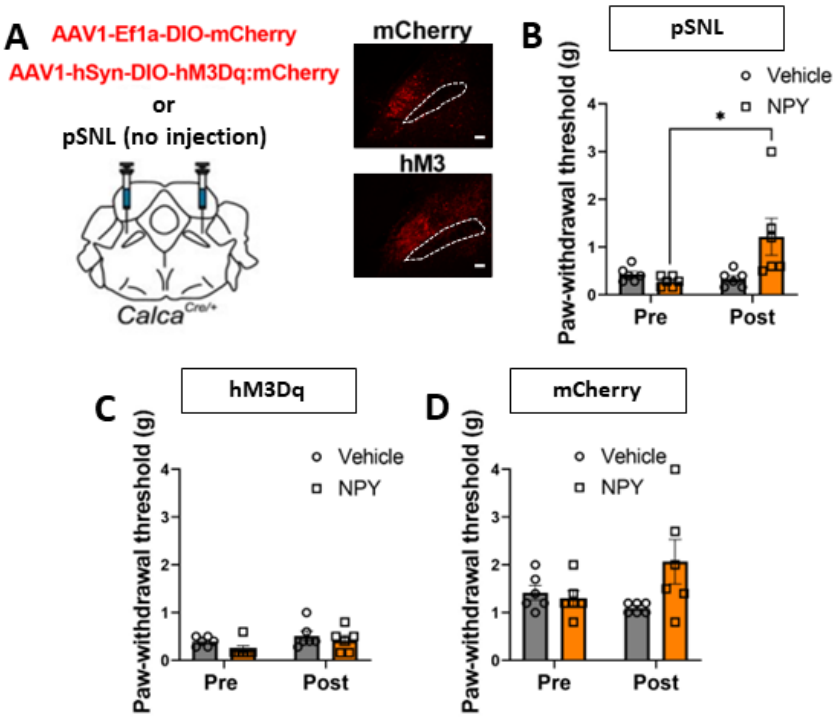

Figure 7. Intrathecal NPY does not reverse hM3Dq/CNO-driven allodynia.

(A) pSNL or bilateral injections of AAV1-Ef1a-DIO-mCherry or AAV1-hSyn-DIO-hM3Dq:mCherry into the PBN of *Calca*$^{cre/+}$ mice. Representative images show expression of mCherry and hM3Dq. Scale bar = 100 µm, dotted line marks the SCP, anterior-posterior Bregma level = -5.1.
(B) Intrathecal (i.t.) injection of NPY^{Leu,Pro} into pSNL animals reversed pSNL driven allodynia.
(C) I.t. injection of NPY^{Leu,Pro} into *Calca*^{Cre}:hM3Dq animals treated with CNO for 3 days did not reverse allodynia.
(C) I.t. injection of NPY^{Leu,Pro} into control *Calca*^{Cre}:mCherry animals treated with CNO for 3 days did not affect the paw-withdrawal threshold.
(B-D) Significance tested by ANOVA with multiple comparisons. * = P < 0.05, ** = P < 0.01, *** = P < 0.001, **** = P < 0.0001. Error bars = SEM.

same mechanisms as nociplasticity driven by pSNL. $NPY^{Leu,Pro}$ injections had not effect on baseline paw withdrawal threshold (Fig. 7D).

Discussion

In addition to the increase in intrinsic excitability of Calca neurons following pSNL and direct chemogenetic stimulation, *Calca* neurons exhibit nociplasticity in the form of an increase in the number of neurons responsive to innocuous tactile stimulation several days after NTG exposure. These effects on excitability and population responsivity may initiate and maintain a persistent pain state given that Calca neurons are necessary for the induction and maintenance of chronic neuropathic pain. However, our data showing that hM4Di inhibition 30 days following pSNL does not reverse allodynia, suggest that *Calca* neurons are not the only site of nociplasticity 30 days after pSNL. We suggest that long-lasting allodynia also involves nociplastic changes in the circuitry downstream of *Calca* neurons (Qi et al., 2022; Zhou et al., 2023; Cai et al., 2014; Wilson et al., 2019; Chen et al., 2017) possibly including the spinal microcircuitry. Chronic pain after sciatic nerve injury changes the microcircuitry of the dorsal horn, allowing Aβ fibers to indirectly stimulate spino-parabrachial projection neurons via a neural circuit that is inhibited under non-painful conditions (Cao et al., 2022; Nelson et al., 2022; Peirs et al., 2021; Boyle et al., 2019; Petitjean et al., 2015; Lu et al., 2013; Todd et al., 2010). Intrathecal injection of neuropeptide Y (NPY) can reverse neuropathic pain (Nelson et al., 2022; Nelson et al., 2021), a result that we confirmed in the pSNL model. However, NPY did not ameliorate the tactile allodynia that develops after hM3Dq/CNO activation of *Calca* neurons,

suggesting that neuroplasticity that promotes allodynia after pSNL is distinct from that that occurs after *Calca*-mediated allodynia.

Supplemental Figures

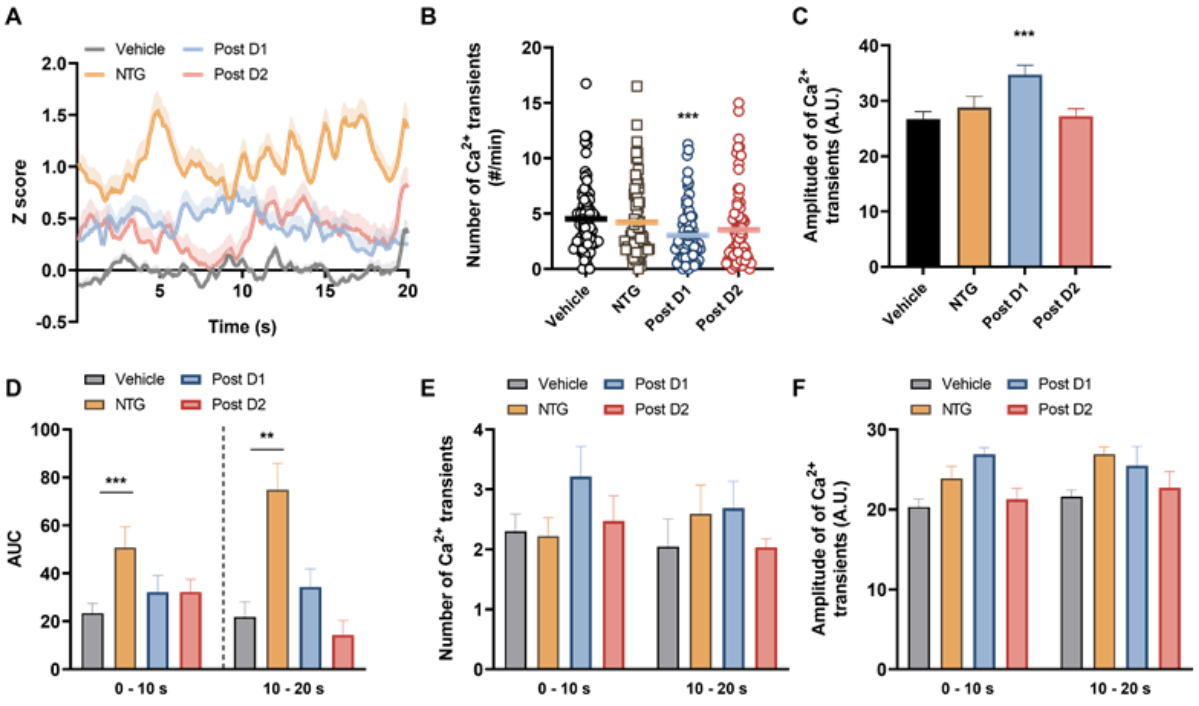

Figure S6. NTG injection does not affect the total number of or amplitude of calcium transients in *Calca* neurons. (Related to Figure 6)

(A) Average traces of individual neurons during baseline period (10 min before von Frey filament application). Shaded area indicates. +S.E.M.
(B) Number of Ca2+ transients during 10 min of baseline.
(C) Amplitude of Ca2+ transients during 10 min of baseline.
(D) Average AUC of individual neurons evoked by von Frey filament. Bar indicates mean S.E.M.
(E) Number of Ca2+ transients during 10 min of baseline.
(F) Peak amplitude during 20 sec of post stimulation period.
(A-F) n = 3 animals, 79 neurons.

Conclusions

The goal of this thesis is to delineate the role PBN *Calca* neurons play in the manifestation of nociplasticity and propose a potential model for the study of nociplastic pain. Previous work in the lab had demonstrated that *Calca* neurons are activated by a wide range of aversive stimuli, are necessary for expression of aversive behavioral phenotypes, and play a key role in aversive learning. The experiments described here extended these studies by demonstrating that:

1. pSNL drives nociplasticity in the form of bilateral allodynia following unilateral injury.
2. *Calca* neurons are activated acutely following neuropathic injury.
3. pSNL drives nociplasticity in the form of increased intrinsic excitability of *Calca* neurons.
4. *Calca* neurons are necessary for the manifestation of neuropathic injury-driven allodynia.
5. *Calca* neurons are necessary for the maintenance of neuropathic injury-driven allodynia.
6. *Calca* gene products are not necessary for the manifestation of pSNL-driven allodynia.
7. Nociplasticity likely occurs downstream of *Calca* neurons.
8. *Calca* neuron activity is sufficient to drive nociplastic pain.
9. Chronic stimulation of *Calca* neurons produces a persistent increase in the intrinsic excitability of *Calca* neurons.

10. *Calca* gene products are not necessary for the manifestation of *Calca* neuron driven nociplasticity.
11. The persistence of nociplastic pain following *Calca* neuron activation is dependent upon the duration of *Calca* neuron activation.
12. Chronic exposure to aversive stimuli across a range of stimulus modalities can produce nociplastic pain via the activation of *Calca* neurons.
13. Robust stimulation of *Calca* neurons increases the basal activity of the *Calca* neuron population that persists for several days.
14. Robust stimulation of *Calca* neurons increases the number of *Calca* neurons that respond to innocuous tactile stimulation.
15. The allodynia induced by activation of *Calca* neurons does not rely on the same spinal microcircuitry that produces neuropathic injury-driven allodynia.

Future Directions

These experiments show that PBN *Calca* neurons are necessary for the manifestation, but not the maintenance, of chronic neuropathic pain, that *Calca* neuron activity is sufficient to drive nociplasticity, and that *Calca* neurons exhibit neuroplasticity following activation. However, the downstream nodes of the nociplasticity circuitry remain unknown. *Tph2* expressing neurons in the RVM exert a nociplastic effect like that of PBN *Calca* neurons when chronically activated (Chen et al., 2019). It would be revealing to determine if there is a direct or indirect connection between PBN *Calca* neurons and this RVM population. The existence of a connection between these two populations could be initially investigated by injecting a Cre-dependent fluorophore conjugated to synaptophysin into the PBN of $Calca^{Cre}$ animals and examining RVM tissue for the colocalization of *Tph2* and the conjugated synaptophysin. A direct connection between PBN *Calca* neurons and RVM *Tph2* neurons could then be established using the progeny of a $Calca^{Flp}$ and $Tph2^{Cre}$ cross. Injecting a Flp-dependent channel rhodopsin into the PBN and a Cre-dependent fluorophore into the RVM would allow for the stimulation of *Calca* terminals in the RVM and electrophysiological recordings from *Tph2* neurons in the RVM. If this experiment does not yield a positive result, the possibility of a two- synapse connection could be examined using the same genetic cross detailed above. Injecting a Flp-dependent fluorophore conjugated to synaptophysin into the PBN and a retrograde traveling Cre-dependent virus that expresses a fluorophore into the RVM of a $Calca^{Flp}$ x $Tph2^{Cre}$ animal would reveal if there were any neurons in the CNS that receive input from PBN *Calca* neurons and project to RVM *Tph2* neurons. It also is possible that these neuronal populations are separated by more than two synapses or that they are part of

entirely parallel circuits despite sharing a function. If this is the case, all the experiments detailed above would produce negative data.

Calca neurons project to several cortical and subcortical nuclei, all of which may be capable of driving nociplasticity. One major target of *Calca* projections is the central nucleus of the amygdala (CeA), which has already been broadly implicated in the experience of chronic pain (Allen et al., 2023; Torres-Rodriguez et al., 2023; Singh et al., 2022; Wilson et al., 2019). Chronic optogenetic stimulation of *Calca* neuron terminals in the CeA may reveal a role for this nucleus in the manifestation of nociplastic pain. However, transient stimulation of CeA projecting PBN neurons only produces transient allodynia (Torres-Rodriguez et al., 2023). This suggests that other structures downstream of the PBN may be involved in the nociplastic phenomenon reported in this thesis. As such, chronic terminal stimulation experiments could also be repeated for all major projection targets of PBN *Calca* neurons. For instance, chronic stimulation of a pain activated subset of dorsomedial prefrontal cortex (dmPFC) neurons also produces persistent allodynia (Qi et al., 2022). Whether this population is downstream of PBN *Calca* neurons is unknown, however *Calca* neurons do appear to project to this region (Pauli et al., 2023). If chronic *Calca* terminal stimulation via ChR2 in the dmPFC produced persistent allodynia, further study of this circuitry would be warranted.

We demonstrated that *Calca*-negative neurons within the PBN also exhibit and increase in *Fos* induction acutely following pSNL, but it is unclear whether these neurons play a role in nociplastic pain. Performing a pSNL on *Calca*^{Tdt} animals and then patching onto Tdt negative neurons would reveal possible changes in the electrophysiology of *Calca* negative neurons in a state of chronic pain. These neurons could also be isolated

by crossing a *Calca*^{Flp} animal to a *Fos*$^{2A\text{-}iCreER}$ animal, coincidentally exposing the progeny of this cross to a transient aversive stimulus and tamoxifen, then injecting a Cre-on Flp-off virus carrying effector genes for the excitation or inhibition of this population into the PBN. Determining how these *Calca* negative neurons behave following the induction of nociplastic pain via the direct stimulation of *Calca* neurons would also provide valuable information regarding the role *Calca* negative neurons play in nociplastic pain. Coinjecting a non-specific GCaMP carrying virus and a Cre-dependent hM3Dq carrying virus into the PBN, then implanting an endoscopic lens over the PBN would reveal any population level changes in the basal and elicited activity of *Calca* negative neurons in a nociplastic pain state.

Finally, we observed that *Calca* neurons exhibit nociplastic change following robust stimulation. Identifying changes in gene expression that could account for the observed physiological changes would be valuable. Injecting Cre-dependent hM3Dq into the PBN of *Calca*^{cre} animals, chronically administering CNO, performing RNAseq on the PBN of these animals, and comparing the mRNA expression profile to that of sham-treated animals would show what genes are up or downregulated in the PBN following the induction of nociplastic pain. Any genes that are up or down-regulated could then be knocked out or overexpressed to determine if their expression level is necessary or sufficient to induce nociplastic pain. Additionally, the expression of immediate early genes could be used to identify clusters of neurons within the PBN that exhibit elevated or depressed activity in a nociplastic pain state. This information could then be used to perform more refined excitation or inhibition of neuronal populations within the PBN.

Methods

Mice

All experiments followed protocols approved by the Institutional Animal Care and Use Committee at the University of Washington and were in accordance with the National Institute of Health guidelines for animal research. Experiments on wild-type animals used C57BL/6 mice. Most experiments used heterozygous *Calca*$^{Cre/+}$ or homozygous *Calca*$^{Cre/Cre}$ mice on a C57BL/6 genetic background were generated and maintained as described (Carter et al., 2013). One set of experiments used *Slc17a6*$^{Cre/+}$ or *Oprm1* $^{Cre/+}$ mice. Male and female animals were 7 to 9 weeks of age at the onset of all experiments and no more than 18 weeks by their experimental endpoint. Before surgical manipulation animals were group housed, had *ad libitum* access to food and water, and were kept on a 12-h, light-dark cycle at 22°C. After surgical manipulation animals were singly housed, all other housing parameters remained consistent. All experiments included 4-10 experimental animals (e.g., transduced with viruses allowing Cre-dependent expression of hM3Dq, hM4Di, ChR2, TeTx) and 4-7 control animals (e.g., transduced with mCherry or YFP) to account for potential variation between experimental sessions. Animals from the same litter were randomly assigned to experimental or control groups. All experiments were performed blind, except the *Oprm1*$^{Cre/+}$ experiment. Individual cohorts of mice were used for all experiments except those mentioned below. The same cohort of *Calca*$^{Cre/+}$:TeTx animals was used in the NTG and cisplatin experiments with 1 week of recovery between NTG and cisplatin injections. The same cohort of *Calca*$^{Cre/+}$:ChR2 animals was used for all ChR2 experiments with 1 week of recovery between the 1-day ChR2 stimulation and

the 5-day ChR2 stimulation experiment. Viral transduction was assessed at the end of each experiment histologically and only mice with correct expression were included in data analysis.

Virus production

AAV1-Ef1a-DIO-mCherry and AAVDJ-SYN-DIO-hM3Dq:mCherry DNA plasmids were provided by B. Roth (Addgene #50462 and #44361). AAV1-SYN-DIO-YFP and AAV1-Ef1a-DIO-ChR2:mCherry DNA plasmids were provided by K. Diesseroth (Stanford University). AAVDJ-Ef1a-DIO-GFP:TeTx and AAV1-CBA-DIO-hM4Di:YFP plasmids were constructed by R. Palmiter (University of Washington). AAV1-CBA-DIO-GCaMP6m DNA plasmid was provided by L. Zweifel. AAV1 serotype viruses were prepared in-house by transfecting HEK cells with each of these plasmids. Viruses were purified by sucrose and CsCl gradient centrifugation steps and re-suspended in 0.1 M phosphate-buffered saline (PBS) at about 10^{13} viral particles/mL. AAVDJ serotype viruses were prepared by Janelia Viral Tools lab.

Partial sciatic nerve ligation

Partial sciatic nerve ligation (pSNL**)** was performed as described (Abraham et al., 2020). In brief, mice were anesthetized with 2% isoflurane at a flow rate of 1 L/min. Subsequently, a 2-cm incision was made over the lateral aspect of the proximal third of the left hind leg. Blunt dissection was used to visualize the sciatic nerve, which was then exteriorized with hooked forceps. For sham surgeries, the sciatic nerve was then immediately returned to its position. For nerve ligation surgeries, a 6-0 silk suture was

passed through 30-50% of the nerve bundle, before being tightly ligated and crushed. The skin was then closed with 6-0 silk sutures.

Intrathecal injection of NPY

Intrathecal injection of [Leu^{31}, Pro^{34}]-NPY (TOCRIS) was performed as described by Nelson et al. (2022). In brief, a 30G needle attached to a 25 µL microsyringe (Hamilton) was inserted between the L5/L6 vertebrae, puncturing the dura mater; 5 µL of vehicle (0.9 % saline) or NPY was injected. Each mouse was injected twice, once with vehicle and once with NPY, with 48 h between injections.

Stereotaxic surgery

Mice were anesthetized with 2% isoflurane at a flow rate of 1 L/minute. After anesthesia induction mice were placed on a stereotaxic frame (David Kopf Instruments). Stereotaxic coordinates in the anterior posterior plane were normalized using a correction factor (F = (Bregma – Lambda)/4.21). Viral injections were performed bilaterally for all experiments into the PBN (anterior-posterior: -1.3, rostral-caudal: -4.8, medial-lateral: +/-1.3) at a rate of 0.2 µL/min for 2.5 min for a total of 0.5 µL. At the end of each experiment animals were euthanized with phenobarbital and the brain was extracted for histological evaluation of viral placement and fiber optic placement.

For *in vivo* Ca^{2+} imaging experiments, viral injections were in the external lateral part of the parabrachial nucleus (PBel) using the following coordinates relative to bregma at the skull surface: AP -4.90 mm; ML ±1.35 mm; DV +3.40. Viruses were injected unilaterally (randomly assigned) 0.5 µl at 0.1 ml/min. A gradient refractive index (GRIN) lens was positioned above the target area (AP -4.80 mm; ML ±1.7 mm; DV +3.65), and

three tungsten wires protruding approximately 0.5 mm beyond the lens surface (A-M systems) were attached to the lens to reduce motion artifacts during imaging. The lens was then lowered at a rate of 0.1 mm/min. To secure the lens to the skull, super glue (C&B Metabond from Parkell) and dental cement were used. After 4 weeks of recovery, mice were tested to ensure field of view (FOV). Animals with a stable FOV were used in the experiments for the subsequent 2-4 weeks.

Allodynia assays

The von Frey, tactile-sensitivity assay was performed using the ascending application method as described (Abraham et al., 2020). Each animal was placed in a 11.5-cm by 7.5-cm chamber with a wire mesh floor (Bioseb). Animals were acclimated to the chamber for 30 min before the assay began. Filaments were applied to the plantar surface of each hind paw a total of 5 times. Filament application began with a 0.16-g filament and ended after two consecutive filaments elicit a paw withdrawal on 3 or more out of 5 applications. The paw-withdrawal thresholds for each hind paw were measured and averaged because there was no significant difference in the left/right paw-withdrawal thresholds following any of the performed manipulations (pSNL, NTG, LiCl, etc.).

The Hargreaves thermal-sensitivity assay was performed as described (Wilson et al., 2019). Each animal was placed in an 11.5-cm by 7.5-cm chamber with a wire mesh floor. Animals were acclimated to the chamber for 30 min before the assay began. Each animal received infrared thermal stimulation (Ugo Basil, model 37370) a total of 3 times on both hind paw plantar surfaces. Latency to paw withdrawal was averaged across the 3 sessions. The paw-withdrawal latency for each paw was averaged as we did not see a difference in their response latency values.

The hot-plate assay was performed as described (Nelson et al., 2022). Each animal was placed in a 16.5-cm by 16.5-cm chamber on a 55°C hot plate (Bioseb) for 30 s. Each animal's total number of nocifensive behaviors on the plate (paw flicks or licks, and jumps) was recorded.

Anxiety and depression assays

The open-field assay was performed as described[31]. Each animal was placed in a 40-cm by 40-cm white plexiglass chamber for 10 min. The sessions were recorded using a USB camera attached to a personal computer. Locomotor and center time data were collected using Ethovision (Noldus).

The elevated-plus-maze assay was performed as described[31]. The custom-made EPM consisted of two sets of crossed arms (two arms enclosed by 30 cm tall transparent plexiglass, two arms open), each 50-cm long , 8-cm wide, and set 65-cm above the floor. Mice were allowed to explore the arena for 10 min. The sessions were recorded by a USB camera attached to a personal computer and were analyzed using EthoVision (Noldus).

The tail-suspension test was performed by suspending each animal by the tail using laboratory tape for one minute. The sessions were recorded by a USB camera attached to a personal computer and were manually scored for freezing behavior by a blinded experimenter.

The sucrose-preference test was performed by housing the animals in caging systems adapted to hold two sipper bottles. The animals were water restricted for 12 h prior to the experiment during the dark cycle. After water restriction, they were

presented with two sipper bottles, one with water and one with 1% sucrose solution. The total fluid consumption from each sipper bottle over a 2-h access period was measured.

Pharmacological injections

Clozapine N-oxide (RTI), nitroglycerin (American Regent Inc.), cisplatin (West Ward) and saline or vehicle controls were injected at 10 mL/kg body weight. CNO was administered at 1 mg/kg for hM3Dq experiments and 5 mg/kg for hM4Di experiments, nitroglycerin at 10 mg/kg, cisplatin at 2.3 mg/kg and saline at 0.9% sodium chloride; vehicle for nitroglycerine was 6 % propylene glycol 6 % ethanol and saline. Lithium chloride (Fisher Scientific) and the saline control for this condition were injected at 15 mL/kg. Lithium chloride was administered at 0.2 M and the saline was 0.9% sodium chloride. All paw-withdrawal measurements were made 2 h after each CNO injection and daily thereafter unless otherwise indicated.

Optogenetic stimulation

After recovery from surgery, mice were acclimated to fiber-optic cable attachment. For von Frey, allodynia assessment, light-pulse trains (20 Hz; 2 s “on”, 2 s “off”) were delivered for 5 or 20 min as described in the text. Stimulation paradigms were programmed using a Master8 (AMPI) pulse stimulator that controlled a blue-light laser (473 nm; LaserGlow). The power of light exiting each side of the branching fiber-optic cable was adjusted to 10 ± 1 mW. All paw-withdrawal measurements were made 2 h after each ChR2 stimulation and daily thereafter

Immunohistochemistry

Mice were anesthetized with phenobarbitol (0.2 ml, i.p.; Akorn) and perfused transcardially with phosphate-buffered saline (PBS) followed by 4% paraformaldehyde (PFA, Electron Microscopy Sciences) in PBS. Brains were post-fixed overnight in 4% PFA at 4°C, cryoprotected in 30% sucrose, frozen in OCT compound (ThermoFisher), and stored at -80°C. Coronal sections (30 µm) were cut on a cryostat (Leica Microsystems) and collected in cold PBS. For immunohistochemistry experiments, sections were washed three times in PBS with 0.2% Triton X-100 (PBST) for 5 min and incubated in a blocking solution (3% normal donkey serum in PBST) for 1 h at room temperature. Sections were incubated overnight at 4°C in PBS with primary antibodies including: chicken-anti-GFP (1:10000, Abcam, ab 13970) or rabbit-anti-dsRed (1:1000, Tacara, ab 632496). After 3 washes in PBS, sections were incubated for 1 h in PBS with secondary antibodies: Alexa Fluor 488 donkey anti-chicken or Alexa Fluor 594 donkey anti-rabbit (1:500, Jackson ImmunoResearch). Tissue was washed 3 times in PBS, mounted onto glass slides, and coverslipped with Fluoromount-G (Southern Biotech). Fluorescent images were acquired using a Keyence BZ-X700 microscope. Images were minimally processed using ImageJ software (NIH) to enhance brightness and contrast for optimal representation of the data. All digital images were processed in the same way between experimental conditions to avoid artificial manipulation between different datasets.

RNAscope *in situ* hybridization

Mice were anesthetized with phenobarbital (0.2 ml, i.p.) then decapitated. Brains were rapidly frozen on crushed Dry Ice. Coronal sections (20 µm) were cut on a cryostat (Leica Microsystems), mounted onto glass slides, and stored at –80°C. RNAscope fluorescent

multiplex assay was performed following the manufacturer's protocols (ACD Biotechne). Samples were taken from 2 males and 2 females in each group (3 and 30 day) and several levels of the PBN were imaged for each animal using a Keyence BZ-X710 microscope. Using the superior cerebellar peduncle (scp) as the center point, images were acquired at 20x in a 3×3 grid, then stacked and stitched together using Fiji for an initial total of 116 PBNs. Images of probe staining within the four-channel sets were subtracted from one another using Fiji's image calculator function to remove background autofluorescence and minimally processed to enhance brightness and contrast for optimal representation of the data. After image optimization, due to difficulty in getting precisely matching bregma levels during sectioning, PBN anatomy was evaluated using fiber-tract location and general structure to categorize the images into two groups. "Rostral" sections were defined by the presence of the caudal part of the nucleus of the lateral lemniscus (NLL) and a more triangular shape of the lateral PBN (Bregma -4.95 to -5.15), and "middle" sections were defined by the presence of the longer central part of the ventral spinocerebellar tract (sctv) and narrower oval appearance of lateral PBN (Bregma 5.15 to -5.35). Sections that were deemed to be further rostral or caudal of these two categories, and sections that had tissue damage in the PBN, were removed for a final count of 89 PBN images. Images were imported into QuPath and a region of interest was drawn over the lateral PBN using the surrounding fiber tracts and brain structure as a guide. RNA expression was quantified by thresholding using the subcellular detection function in QuPath. Cells were deemed positive for *Calca* or *Cck* if they had 5 or more puncta and cells were deemed positive for *Fos* if they had 4 or more puncta because

Calca and *Cck* had denser transcript labeling. An average of ~1700 DAPI-positive cells were analyzed for each section for a total of ~150,000 cells analyzed.

Electrophysiology

Mice were deeply anesthetized with Euthasol (i.p. 1 µl per 10 g body weight) and intracardially perfused with ice-cold cutting solution containing (in mM): 92 N-methyl-D-glucamine, 25 D-glucose, 2.5 KCl, 10 $MgSO_4$, 1.25 NaH_2PO_4, 30 $NaHCO_3$, 0.5 $CaCl_2$, 20 HEPES, 2 thiourea, 5 Na-ascorbate, 3 Na-pyruvate. Brains were quickly removed after perfusion and 250-□m coronal slices were prepared (Leica VT1200) in the same ice-cold solution. Brain slices were kept in the cutting solution at 33°C for 10 min and then transferred to a room temperature recovery solution containing (in mM): 13 D-glucose, 124 NaCl, 2.5 KCl, 2 $MgSO_4$, 1.25 NaH_2PO_4, 24 $NaHCO_3$, 2 $CaCl_2$, 5 HEPES for at least 1 h. Slices were individually transferred to 33°C artificial cerebral spinal fluid containing (in mM): 11 D-glucose, 126 NaCl, 2.5 KCl, 1.2 NaH_2PO_4, 26 $NaHCO_3$, 2.4 $CaCl_2$, 1.2 $MgCl_2$ for recording. All solutions were saturated with 95% O2/5% CO2 and adjusted to pH 7.3–7.4, 300–310 mOsm.

Epifluorescence microscope (OLYMPUS BX51WI) was used to visualize *Calca* neurons expressing AAV-DIO-hM3Dq-mCherry and AAV-DIO-mCherry. A 3-5 MΩ glass pipet containing (in mM): 135 K-gluconate, 4 KCl, 10 HEPES, 4 Mg-ATP, 0.3 Na-GTP (pH 7.35, 280 -300 mOsm) was used to record neuron activity. To record intrinsic firing frequencies, 800-ms current injections with 20-pA steps from -100 pA to 240 pA were applied in current clamp, with initial holding potential at -70 mV and repeated every 10 s. To record the efficiency of CNO application, cell-attached measurement was used to

record action potential in voltage clamp with 0 pA holding current. CNO (3 µM) was bath applied after 3 min of action potential firing. All data were obtained using MultiClamp 700B amplifier (Molecular Devices). Data acquisition and analysis were done using pClamp 11 and Clampfit 11.0.3.

Calcium imaging

AAV-Ef1a-DIO-GCaMP6m was injected into the PBN of *Calca*$^{Cre/+}$ mice. After 6 weeks of recovery, the nVista (Inscopix) microscope was attached and connected once a week to check the field of view. Recording was conducted using the IDAS program (Inscopix), and the best focus was determined through visual inspection. Occasionally, the mice received a brief air puff as an aversive stimulus. For multi-day imaging of *Calca* neurons, nVista was connected Ethovision (Noldus) via BNC cable to synchronize video recording and Ca^{2+} imaging to ensure that the onset and offset of the Ca^{2+} imaging session matched the video recording. The microendoscope was connected to a commutator (Inscopix) and attached to the baseplate on the mouse, which was then housed in an open-top cage for 4 days to maintain the same field of view throughout the experimental period.

On day 1, a vehicle solution (6 % propylene glycol 6 % ethanol and saline) was injected intraperitoneally, and the mouse was placed in the von Frey-stimulation chamber for a 45-min acclimation. The imaging session consisted of 5 min of basal activity and 10 min of von Frey stimulation. During the von Frey-stimulation sessions, the mouse was exposed to 8 stimulations of 0.4-g von Frey filament with 1-min, inter-trial intervals. After the imaging session, the LED was turned off, but the microendoscope remained connected, and the mouse was then returned to open-top cage until the start of the next day's experiment. On day 2, NTG (10 mg/kg, dissolved in 6 % propylene glycol 6 %

ethanol and saline) was injected intraperitoneally. The same imaging session as on day 1 was repeated. On days 3 and 4, the mice were placed in the von Frey-stimulation chamber for imaging as on previous days.

The imaging parameters had insignificant photobleaching, but sufficient fluorescence (LED power, 0.2 - 0.4; sampling rate 10 Hz). The raw data were processed using IDPS software (ver. 1.9.1, Inscopix). All images acquired over 4 days were concatenated for further analysis. After applying 4X spatial and 2X temporal downsampling, the data underwent spatial bandpass filtering to reduce background noise. Subsequently, motion correction was applied to the images based on a reference frame and region of interest (ROI) within the field of view (FOV). Using IDPS, ΔF/F movies were generated, and then PCA/ICA analysis was performed to extract neuronal activities. In cases where there was significant motion or higher background noise, a manual ROI analysis method was employed. To do that, the maximum projection images were used as a reference for spatial information of the neurons, and ROIs were manually drawn based on the borders of the neurons. All neurons analyzed using PCA/ICA and manual ROI methods were visually inspected for each cell, taking into consideration their shape and dynamics, to ensure accuracy.

The outputs of PCA/ICA (ΔF/F) were processed using customized MATLAB code to calculate the Z-score. In the case of manual ROI analysis, ΔF/F was calculated as ΔF/F=(F−Fmean)/Fmean. Fmean indicates mean fluorescent during the day 1 baseline. For basal activity analysis, concatenated Ca^{2+} traces were used to calculate the Z-score, and the Z-scored data were compared across days using the formula: Z=(F−Fmean)/Fstd. Fstd indicates the standard deviation of fluorescent during the day 1 baseline. For the

analysis of von Frey filament-elicited responses, the traces from -20 s to 20 s were extracted and used to calculate the Z-scores. To compare the fluorescent responses, all data points were calculated relative to the -20 s to 0 s periods because the mice exhibited different basal activities every day due to intraperitoneal injections or allodynia.

Responsive neurons were identified through statistical analysis comparing the area under the curve (AUC) of pre- and post-stimulation. The AUCs were calculated for three time blocks (-5 to 0 s, 0 to 5 s, and 5 to 10 s) across 8 trials and compared using the Wilcoxon Signed-rank test. Neurons were classified as "increased" if there was a significant increase in the AUC in more than one post-stimulation block. If neither post-stimulation block showed statistical significance, neurons were classified as "unresponsive". Neurons that exhibited a statistically significant decrease in activity across two blocks were classified as "decreased".

Quantification and statistical analysis

Data were analyzed in GraphPad Prism 9.5.1 (Graphpad Software) by two-way ANOVA with Šidák post hoc correction; for longitudinal assays Bonferroni's multiple comparisons correction was applied; $p < 0.05$ was deemed statistically significant. All data are presented as the mean ± standard error of the mean (SEM). The asterisks in the figures represent the p values of post hoc tests corresponding to the following values * $p < 0.05$, ** $p < 0.01$, *** $p < 0.001$, **** $p < 0.0001$. Following histology and imaging, any mouse whose targeted injection site was wrong was excluded from experimental analysis.

References

Abraham A.D., Leung E.J.Y., Wong B.A., Rivera Z.M.G., Kruse L.C., Clark J.J., Land B.B. (2020). Orally consumed cannabinoids provide long-lasting relief of allodynia in a mouse model of chronic neuropathic pain. Neuropsychopharmacology 45, 1105-1114. https://doi.org/10.1038/s41386-019-0585-3.

Alhadeff A.L., Su Z., Hernandez E., Klima M.L., Phillips S.Z., Holland R.A., Guo C., Hantman A.W., De Jonghe B.C., Betley J.N. (2018). A neural circuit for the suppression of pain by a competing need state. Cell 173, 140-152. https://doi.org/10.1016/j.cell.2018.02.057.

Allen H.N., Chaudhry S., Hong V.M., Lewter L.A., Sinha G.P., Carrasquillo Y., Taylor B.K., Kolber B.J. (2023). A parabrachial-to-amygdala circuit that determines hemispheric lateralization of somatosensory processing. Biol. Psychiatry. 93, 370-381. https://doi.org/10.1016/j.biopsych.2022.09.010.

Arguis M.J., Perez J., Martínez G., Ubre M., Gomar C. (2008). Contralateral neuropathic pain following a surgical model of unilateral nerve injury in rats. Reg. Anesth. Pain Med. 33, 211-216. https://doi.org/10.1016/j.rapm.2007.12.003.

Arthurs J.W., Bowen A.J., Palmiter R.D., Baertsch N.A. (2023). Parabrachial tachykinin1-expressing neurons involved in state-dependent breathing control. Nat Commun. 14, 963. https://doi.org/10.1038/s41467-023-36603-z.

Arthurs J.W., Pauli J.L., Palmiter R.D. (2023). Activation of parabrachial tachykinin 1 neurons counteracts some behaviors mediated by parabrachial calcitonin gene-related peptide neurons. Neuroscience 517, 105-111. https://doi.org/10.1016/j.neuroscience.2023.03.003.

Ballantyne J., Shin N. (2008). Efficacy of opioids for chronic pain: a review of the evidence. Clin J Pain 24(6):469-78. https://doi.org/10.1097/AJP.0b013e31816b2f26.

Barik A., Sathyamurthy A., Thompson J., Seltzer M., Levine A., Chesler A. (2021). A spinoparabrachial circuit defined by Tacr1 expression drives pain. Elife 10:e61135. https://doi.org/10.7554/eLife.61135.

Basbaum A.I., Bautista D.M., Scherrer G., Julius D. (2009). Cellular and molecular mechanisms of pain. Cell 139(2):267-84. https://doi.org/10.1016/j.cell.2009.09.028.

Bernard J.F., Dallel R., Raboisson P., Villanueva L., Le Bars D. (1995). Organization of the efferent projections from the spinal cervical enlargement to the parabrachial area and periaqueductal gray: a PHA-L study in the rat. J Comp Neurol. 353(4):480-505. https://doi.org/10.1002/cne.903530403.

Bourgeais L., Gauriau C., Monconduit L., Villanueva L., Bernard J.F. (2003). Dendritic domains of nociceptive-responsive parabrachial neurons match terminal fields of lamina I neurons in the rat. J Comp Neurol 464(2):238-56. https://doi.org/10.1002/cne.10793.

Bowen A.J., Chen J.Y., Huang Y.W., Baertsch N.A., Park S., Palmiter R.D. (2020). Dissociable control of unconditioned responses and associative fear learning by parabrachial CGRP neurons. Elife 9:e59799. https://doi.org/10.7554/eLife.59799.

Boyle K.A., Gradwell M.A., Yasaka T., Dickie A.C., Polgár E., Ganley R.P., Orr D.P.H., Watanabe M., Abraira V.E., Kuehn E.D., Zimmerman A.L., Ginty D.D., Callister R.J., Graham B.A., Hughes D.I. (2019). Defining a spinal microcircuit that gates myelinated afferent input: implications for tactile allodynia. Cell Rep. 28, 526-540. https://doi.org/10.1016/j.celrep.2019.06.040.

Busse J.W., Wang L., Kamaleldin M., Craigie S., Riva J.J., Montoya L., Mulla S.M., Lopes L.C., Vogel N., Chen E., Kirmayr K., De Oliveira K., Olivieri L., Kaushal A., Chaparro L.E., Oyberman I., Agarwal A., Couban R., Tsoi L., Lam T., Vandvik P.O., Hsu S., Bala M.M., Schandelmaier S., Scheidecker A., Ebrahim S., Ashoorion V., Rehman Y., Hong P.J., Ross S., Johnston B.C., Kunz R., Sun X., Buckley N., Sessler D.I., Guyatt G.H. (2018). Opioids for Chronic Noncancer Pain: A Systematic Review and Meta-analysis. JAMA 320(23):2448-2460. https://doi.org/10.1001/jama.2018.18472.

Butler R.K., Finn D.P. (2009). Stress-induced analgesia. Prog. Neurobiol. 88, 184-202. https://doi.org/10.1016/j.pneurobio.2009.04.003.

Cai Y.Q., Wang W., Hou Y.Y., Pan Z.Z. (2014). Optogenetic activation of brainstem serotonergic neurons induces persistent pain sensitization. Mo Pain 10, 70. https://doi.org/10.1186/1744-8069-10-70.

Campos C.A., Bowen A.J., Roman C.W., Palmiter R.D. (2018). Encoding of danger by parabrachial CGRP neurons. Nature 555, 617-622. https://doi.org/10.1038/nature25511.

Campos C.A., Bowen A.J., Han S., Wisse B.E., Palmiter R.D., Schwartz M.W. (2017). Cancer-induced anorexia and malaise are mediated by CGRP neurons in the parabrachial nucleus. Nat. Neurosci. 20, 934-942. https://doi.org/10.1038/nn.4574.

Campos C.A., Bowen A.J., Schwartz M.W., Palmiter R.D. (2016). Parabrachial CGRP neurons control meal termination. Cell Metab. 23, 811-820. https://doi.org/10.1016/j.cmet.2016.04.006.

Cao B., Scherrer G., Chen L. (2022). Spinal cord retinoic acid receptor signaling gates mechanical hypersensitivity in neuropathic pain. Neuron 110, 4108-4124.e6. https://doi.org/10.1016/j.neuron.2022.09.027.

Carter M.E., Han S., Palmiter R.D. (2015). Parabrachial calcitonin gene-related peptide neurons mediate conditioned taste aversion. J. Neurosci. 35, 4582-4586. https://doi.org/10.1523/JNEUROSCI.3729-14.2015.

Carter M.E., Soden M.E., Zweifel L.S., Palmiter R.D. (2013). Genetic identification of a neural circuit that suppresses appetite. Nature 503, 111-114. https://doi.org/10.1038/nature12596.

Chen J.Y., Campos C.A., Jarvie B.C., Palmiter R.D. (2018). Parabrachial CGRP neurons establish and sustain aversive taste memories. Neuron 100, 891-899.e5. https://doi.org/10.1016/j.neuron.2018.09.032.

Chen Q., Roeder Z., Li M.H., Zhang Y., Ingram S.L., Heinricher M.M. (2017). Optogenetic evidence for a direct circuit linking nociceptive transmission through the parabrachial complex with pain-modulating neurons of the rostral ventromedial medulla (RVM). eNeuro 4, ENEURO.0202-17.2017. https://doi.org/10.1523/ENEURO.0202-17.2017.

Chiang M.C., Nguyen E.K., Canto-Bustos M., Papale A.E., Oswald A.M., Ross S.E. (2020). Divergent neural pathways emanating from the lateral parabrachial nucleus mediate distinct components of the pain response. Neuron 106, 927-939.e5. https://doi.org/10.1016/j.neuron.2020.03.014.

Choi S., Hachisuka J., Brett M.A., Magee A.R., Omori Y., Iqbal N.U., Zhang D., DeLisle M.M., Wolfson R.L., Bai L., Santiago C., Gong S., Goulding M., Heintz N., Koerber H.R., Ross S.E., Ginty D.D. (2020). Parallel ascending spinal pathways for affective touch and pain. Nature 587, 258-263. https://doi.org/10.1038/s41586-020-2860-1.

Chung L. (2015). A Brief Introduction to the Transduction of Neural Activity into Fos Signal. Dev. Reprod. 19, 61-67. https://doi.org/10.12717/DR.2015.19.2.061.

Dahlhamer J., Lucas J., Zelaya C., Nahin R., Mackey S., DeBar L., Kerns R., Von Korff M., Porter L., Helmick C. (2016). Prevalence of chronic pain and high-impact chronic pain among adults - United States, 2016. MMWR Morb. Mortal. Wkly. Rep. 67, 1001-1006. https://doi.org/10.15585/mmwr.mm6736a2.

Deng J., Zhou H., Lin J.K., Shen Z.X., Chen W.Z., Wang L.H., Li Q., Mu D., Wei Y.C., Xu X.H., Sun Y.G. (2020). The parabrachial nucleus directly channels spinal nociceptive signals to the intralaminar thalamic nuclei, but not the amygdala. Neuron 107, 909-923.e6. https://doi.org/10.1016/j.neuron.2020.06.017.

Dydyk A.M., Givler A. (2023). Central Pain Syndrome. In: StatPearls [Internet]. Treasure Island (FL): StatPearls Publishing.

Fitzcharles M.A., Cohen S.P., Clauw D.J., Littlejohn G., Usui C., Häuser W. (2021). Nociplastic pain: towards an understanding of prevalent pain conditions. Lancet 397, 2098-2110. https://doi.org/10.1016/S0140-6736(21)00392-5.

Fu X., Sun L., Dong R., Chen J.Y., Silakit R., Condon L.F., Lin Y., Lin S., Palmiter R.D., Gu L. (2022). Polony gels enable amplifiable DNA stamping and spatial transcriptomics of chronic pain. Cell 185, 4621-4633.e17. https://doi.org/10.1016/j.cell.2022.10.021.

Fung H.L., Ogata H., Kamiya A., Maier G.A.. Pharmacokinetics of nitroglycerin after parenteral and oral dosing in the rat. J. Pharm. Sci. 73, 873-879. https://doi.org/10.1002/jps.2600730704.

Grady F., Peltekian L., Iverson G., Geerling J.C. (2020). Direct parabrachial-cortical connectivity. Cereb. Cortex 30, 4811-4833. https://doi.org/10.1093/cercor/bhaa072.

Gauriau C., Bernard J.F. (2002). Pain pathways and parabrachial circuits in the rat. Exp. Physiol. 87, 251-258. https://doi.org/10.1113/eph8702357.

Groenewald C.B., Murray C.B., Palermo T.M. (2020). Adverse childhood experiences and chronic pain among children and adolescents in the United States. Pain Rep. 5, e839. https://doi.org/10.1097/PR9.0000000000000839.

Han S., Soleiman M.T., Soden M.E., Zweifel L.S., Palmiter R.D. (2015). Elucidating an affective pain circuit that creates a threat memory. Cell 162, 363-374. https://doi.org/10.1016/j.cell.2015.05.057.

Hermann G.E., Rogers R.C. (1985). Convergence of vagal and gustatory afferent input within the parabrachial nucleus of the rat. J. Auton. Nerv. Syst. 13, 1-17. https://doi.org/10.1016/0165-1838(85)90002-5.

Huang D., Grady F.S., Peltekian L., Laing J.J., Geerling J.C. (2021). Efferent projections of CGRP/Calca-expressing parabrachial neurons in mice. J. Comp. Neurol. 529, 2911-2957. https://doi.org/10.1002/cne.25136.

Huo J., Du F., Duan K., Yin G., Liu X., Ma Q., Dong D., Sun M., Hao M., Su D., Huang T., Ke J., Lai S., Zhang Z., Guo C., Sun Y., Cheng L. (2023). Identification of brain-to-spinal circuits controlling the laterality and duration of mechanical allodynia in mice. Cell Rep. 42, 112300. https://doi.org/10.1016/j.celrep.2023.112300.

Kang S.J., Liu S., Ye M., Kim D.I., Pao G.M., Copits B.A., Roberts B.Z., Lee K.F., Bruchas M.R., Han S. (2022). A central alarm system that gates multi-sensory innate threat cues to the amygdala. Cell Rep. 40, 111222. https://doi.org/10.1016/j.celrep.2022.111222.

Karthik S., Huang D., Delgado Y., Laing J.J., Peltekian L., Iverson G.N., Grady F., Miller R.L., McCann C.M., Fritzsch B., Iskusnykh I.Y., Chizhikov V.V., Geerling J.C. (2022). Molecular ontology of the parabrachial nucleus. J. Comp. Neurol. 530, 1658-1699. https://doi.org/10.1002/cne.25307.

Kim J.C., Cook M.N., Carey M.R., Shen C., Regehr W.G., Dymecki S.M. (2009). Linking genetically defined neurons to behavior through a broadly applicable silencing allele. Neuron 63, 305-15. https://doi.org/10.1016/j.neuron.2009.07.010.

Koltzenburg M., Wall P.D., McMahon S.B. (1999). Does the right side know what the left is doing? Trends Neurosci. 22, 122-7. https://doi.org/10.1016/s0166-2236(98)01302-2.

Kosek E., Clauw D., Nijs J., Baron R., Gilron I., Harris R.E., Mico J.A., Rice A.S.C., Sterling M. (2021). Chronic nociplastic pain affecting the musculoskeletal system: clinical criteria and grading system. Pain 162, 2629-2634. https://doi.org/10.1097/j.pain.0000000000002324.

Liang S.H., Zhao W.J., Yin J.B., Chen Y.B., Li J.N., Feng B., Lu Y.C., Wang J., Dong Y.L., Li Y.Q. (2020). A neural circuit from thalamic paraventricular nucleus to central amygdala for the facilitation of neuropathic pain. J. Neurosci. 40, 7837-7854. https://doi.org/10.1523/JNEUROSCI.2487-19.2020.

Liu S., Ye M., Pao G.M., Song S.M., Jhang J., Jiang H., Kim J.H., Kang S.J., Kim D.I., Han S. (2021). Divergent brainstem opioidergic pathways that coordinate breathing with pain and emotions. Neuron 110, 857-873.e9. https://doi.org/10.1016/j.neuron.2021.11.029.

Lu Y., Dong H., Gao Y., Gong Y., Ren Y., Gu N., Zhou S., Xia N, Sun Y.Y., Ji. R.R., Xiong L. (2013). A feed-forward spinal cord glycinergic neural circuit gates mechanical allodynia. J. Clin. Invest. 123, 4050–4062. https://doi.org/10.1172/JCI70026.

Ma Q. (2022). A functional subdivision within the somatosensory system and its implications for pain research. Neuron 110, 749-769. https://doi.org/10.1016/j.neuron.2021.12.015.

Maixner W., Fillingim R.B., Williams D.A., Smith S.B., Slade G.D. (2016). Overlapping chronic pain conditions: implications for diagnosis and classification. J. Pain 17, T93-T107. https://doi.org/10.1016/j.jpain.2016.06.002.

Malet M., Leiguarda C., Gastón G., McCarthy C., Brumovsky P. (2017). Spinal activation of the NPY Y1 receptor reduces mechanical and cold allodynia in rats with chronic constriction injury. Peptides 92, 38–45. https://doi.org/10.1016/j.peptides.2017.04.005.

Malmberg A.B., Basbaum A.I. (1998). Partial sciatic nerve injury in the mouse as a model of neuropathic pain: behavioral and neuroanatomical correlates. Pain 76, 215-22. https://doi.org/10.1016/s0304-3959(98)00045-1.

Millan M.J. (2002). Descending control of pain. Prog Neurobiol. 66(6):355-474. https://doi.org/10.1016/s0301-0082(02)00009-6.

Mills S.E.E., Nicolson K.P., Smith B.H. (2019). Chronic pain: a review of its epidemiology and associated factors in population-based studies. Br. J. Anaesth. 123, e273-e283. https://doi.org/10.1016/j.bja.2019.03.023.

Moon H.C., Park Y.S. (2017). Reduced GABAergic neuronal activity in zona incerta causes neuropathic pain in a rat sciatic nerve chronic constriction injury model. J. Pain Res. 10, 1125-1134. https://doi.org/10.2147/JPR.S131104.

Nelson T.S., Sinha G.P., Santos D.F.S., Jukkola P., Prasoon P., Winter M.K., McCarson K.E., Smith B.N., Taylor B.K. (2022). Spinal neuropeptide Y Y1 receptor-expressing neurons are a pharmacotherapeutic target for the alleviation of neuropathic pain. Proc. Natl. Acad. Sci. USA 119, e2204515119. https://doi.org/10.1073/pnas.2204515119.

Nelson T.S., Taylor B.K. (2021). Targeting spinal neuropeptide Y1 receptor-expressing interneurons to alleviate chronic pain and itch. Prog. Neurobiol. 196, 101894. https://doi.org/10.1016/j.pneurobio.2020.101894.

Nestler E.J., Barrot M., Self D.W. (2001). DeltaFosB: a sustained molecular switch for addiction. Proc Natl Acad Sci U S A 25;98(20):11042-6. https://doi.org/10.1073/pnas.191352698.

Nijs J., Lahousse A., Kapreli E., Bilika P., Saraçoğlu İ., Malfliet A., Coppieters I., De Baets L,. Leysen L., Roose E., Clark J., Voogt L., Huysmans E. (2021). Nociplastic pain criteria or recognition of central sensitization? Pain phenotyping in the past, present and future. J Clin. Med. 10, 3203. https://doi.org/10.3390/jcm10153203.

Palmiter R.D. (2018). The parabrachial nucleus: CGRP neurons function as a general alarm. Trends Neurosci. 41, 280-293. https://doi.org/10.1016/j.tins.2018.03.007.

Park H.J., Stokes J.A., Pirie E., Skahen J., Shtaerman Y., Yaksh T.L. (2013). Persistent hyperalgesia in the cisplatin-treated mouse as defined by threshold measures, the conditioned place preference paradigm, and changes in dorsal root ganglia activated transcription factor 3: the effects of gabapentin, ketorolac, and etanercept. Anesth. Analg. 116, 224-31. https://doi.org/10.1213/ANE.0b013e31826e1007.

Pauli J.L., Chen J.Y., Basiri M.L., Park S., Carter M.E., Sanz E., McKnight G.S., Stuber G.D., Palmiter R.D. (2022). Molecular and anatomical characterization of parabrachial neurons and their axonal projections. Elife 11:e81868. https://doi.org/10.7554/eLife.81868.

Peirs C., Williams S.G., Zhao X., Arokiaraj C.M., Ferreira D.W., Noh M.C., Smith K.M., Halder P., Corrigan K.A., Gedeon J.Y., Lee S.J., Gatto G., Chi D., Ross S.E., Goulding M., Seal R.P. (2021). Mechanical allodynia circuitry in the dorsal horn is defined by the nature of the injury. Neuron 109, 73-90.e7. https://doi.org/10.1016/j.neuron.2020.10.027.

Petitjean H., Pawlowski S.A., Fraine S.L., Sharif B., Hamad D., Fatima T., Berg J., Brown C.M., Jan L.Y., Ribeiro-da-Silva A., Braz J.M., Basbaum A.I., Sharif-Naeini R. (2015). Dorsal Horn Parvalbumin Neurons Are Gate-Keepers of Touch-Evoked Pain after Nerve Injury. Cell Rep. 13, 1246–1257. https://doi.org/10.1016/j.celrep.2015.09.080.

Pradhan A.A., Smith M.L., McGuire B., Tarash I., Evans C.J., Charles A. (2014). Characterization of a novel model of chronic migraine. Pain 155, 269-274. https://doi.org/10.1016/j.pain.2013.10.004.

Qi X., Cui K., Zhang Y., Wang L., Tong J., Sun W., Shao S., Wang J., Wang C., Sun X., Xiao L., Xi K., Cui S., Liu F., Ma L., Zheng J., Yi M., Wan Y. (2022). A nociceptive neuronal ensemble in the dorsomedial prefrontal cortex underlies pain chronicity. Cell Rep.41, 111833. https://doi.org/10.1016/j.celrep.2022.111833.

Raper J., Morrison R.D., Daniels J.S., Howell L., Bachevalier J., Wichmann T., Galvan A. (2017). Metabolism and distribution of clozapine-N-oxide: implications for nonhuman primate chemogenetics. ACS Chem. Neurosci. 8, 1570-1576. https://doi.org/10.1021/acschemneuro.7b00079.

Raver C., Uddin O., Ji Y., Li Y., Cramer N., Jenne C., Morales M., Masri R., Keller A. (2020). An amygdalo-parabrachial pathway regulates pain perception and chronic pain. J. Neurosci. 40, 3424-3442. https://doi.org/10.1523/JNEUROSCI.0075-20.2020.

Rodriguez E., Sakurai K., Xu J., Chen Y., Toda K., Zhao S., Han B.X., Ryu D., Yin H., Liedtke W., Wang F. (2017). A craniofacial-specific monosynaptic circuit enables heightened affective pain. Nat. Neurosci. 1734-1743. https://doi.org/10.1038/s41593-017-0012-1.

Saper C.B., Loewy A.D. (1980). Efferent connections of the parabrachial nucleus in the rat. Brain Res. 197, 291-317. https://doi.org/10.1016/0006-8993(80)91117-8.

Saper C.B., Romanovsky A.A., Scammell T.E. (2012). Neural circuitry engaged by prostaglandins during the sickness syndrome. Nat Neurosci. 15(8):1088-95. https://doi.org/10.1038/nn.3159.

Schiavo G., Matteoli M., Montecucco C. (2000). Neurotoxins affecting neuroexocytosis. Physiol. Rev. 80, 717-66. https://doi.org/10.1152/physrev.2000.80.2.717.

Sherman A.L., Morris M.C., Bruehl S., Westbrook T.D., Walker L.S. (2015). Heightened temporal summation of pain in patients with functional gastrointestinal disorders and history of trauma. Ann. Behav. Med. 49, 785-92. https://doi.org/10.1007/s12160-015-9712-5.

Shinohara K., Watabe A.M., Nagase M., Okutsu Y., Takahashi Y., Kurihara H., Kato F. (2017). Essential role of endogenous calcitonin gene-related peptide in pain-associated plasticity in the central amygdala. Eur. J .Neurosci. 46, 2149-2160. https://doi.org/10.1111/ejn.13662.

Singh S., Wilson T.D., Valdivia S., Benowitz B., Chaudhry S., Ma J., Adke A.P., Soler-Cedeño O., Velasquez D., Penzo M.A., Carrasquillo Y. (2022). An inhibitory circuit from central amygdala to zona incerta drives pain-related behaviors in mice. Elife 11:e68760. https://doi.org/10.7554/eLife.68760.

Smith T.J., Hillner B.E. (2019). The Cost of Pain. JAMA Netw Open 2(4):e191532. https://doi.org/10.1001/jamanetworkopen.2019.1532. PMID: 30951152.

Sugimoto M., Takahashi Y., Sugimura Y.K., Tokunaga R., Yajima M., Kato F. (2021). Active role of the central amygdala in widespread mechanical sensitization in rats with facial inflammatory pain. Pain 162, 2273-2286. https://doi.org/10.1097/j.pain.0000000000002224.

Sun L., Liu R., Guo F., Wen M.Q., Ma X.L., Li K.Y., Sun H., Xu C.L., Li Y.Y., Wu M.Y., Zhu Z.G., Li X.J., Yu Y.Q., Chen Z., Li X.Y., Duan S. (2020). Parabrachial nucleus circuit governs neuropathic pain-like behavior. Nat. Commun. 11, 5974. https://doi.org/10.1038/s41467-020-19767-w.

Ta L.E., Low P.A., Windebank A.J. (2009). Mice with cisplatin and oxaliplatin-induced painful neuropathy develop distinct early responses to thermal stimuli. Mol. Pain 5, 9. https://doi.org/10.1186/1744-8069-5-9.

Todd A.J. (2010). Neuronal circuitry for pain processing in the dorsal horn. Nat. Rev. Neurosci. 11, 823-36. https://doi.org/10.1038/nrn2947.

Tokita K., Inoue T., Boughter J.D. Jr. (2009). Afferent connections of the parabrachial nucleus in C57BL/6J mice. Neuroscience 161, 475-88. https://doi.org/10.1016/j.neuroscience.2009.03.046.

Torres-Rodriguez J.M., Wilson T.D., Singh S., Torruella-Suárez M.L., Chaudhry S., Adke A.P., Becker J.J., Neugebauer B., Lin J.L., Martinez Gonzalez S., Soler-Cedeño O., Carrasquillo Y. (2023). The parabrachial to central amygdala pathway is critical to injury-induced pain sensitization in mice. Neuropsychopharmacology. In press. https://doi.org/10.1038/s41386-023-01673-6.

Wilson T.D., Valdivia S., Khan A., Ahn H.S., Adke A.P., Martinez Gonzalez S., Sugimura Y.K., Carrasquillo Y. (2019). Dual and Opposing Functions of the Central Amygdala in the Modulation of Pain. Cell Rep. 29, 332-346.e5. https://doi.org/10.1016/j.celrep.2019.09.011.

Wu P.Y., Yang X., Wright D.E., Christianson J.A. (2020). Foot shock stress generates persistent widespread hypersensitivity and anhedonic behavior in an anxiety-prone strain of mice. Pain 161, 211-219. https://doi.org/10.1097/j.pain.0000000000001703.

Wu Q., Zheng R., Srisai D., McKnight G.S., Palmiter R.D. (2013). NR2B subunit of the NMDA glutamate receptor regulates appetite in the parabrachial nucleus. Proc. Natl. Acad. Sci. USA 110, 14765-70. https://doi.org/10.1073/pnas.1314137110.

Yap P.S., Fung H.L. (1978). Pharmacokinetics of nitroglycerin in rats. J. Pharm. Sci. 67, 584-6. https://doi.org/10.1002/jps.2600670446.

You D.S., Albu S., Lisenbardt H., Meagher M.W. (2019). Cumulative Childhood Adversity as a Risk Factor for Common Chronic Pain Conditions in Young Adults. Pain Med. 20, 486-494. https://doi.org/10.1093/pm/pny106.

Zajdel J., Sköld J., Jaarola M., Singh A.K., Engblom D. (2021). Calcitonin gene related peptide α is dispensable for many danger-related motivational responses. Sci. Rep. 11, 16204. https://doi.org/10.1038/s41598-021-95670-8.

Zhang C., Kaye J.A., Cai Z., Wang Y., Prescott S.L., Liberles S.D. (2021). Area Postrema Cell Types that Mediate Nausea-Associated Behaviors. Neuron 109, 461-472.e5. https://doi.org/10.1016/j.neuron.2020.11.010.

Zhou H., Li M., Zhao R., Sun L., Yang G. (2023). A sleep-active basalocortical pathway crucial for generation and maintenance of chronic pain. Nat. Neurosci. 26, 458-469. https://doi.org/10.1038/s41593-022-01250-y.